

Quantitative evaluation of
magnetisation transfer (MT) in human brain:
Extrapolation from fast pulse repetition
to continuous wave saturation

Andreas Piringer

February 5, 1998

Department of Medical Radiation Physics, Karolinska Intstitutet, Stockholm University

MR Research Centre, Karolinska Sjukhuset, 171 76 Stockholm

e-mail: andreas@mrc.ks.se

Contents

	Page
1. Abstract	3
2. Introduction	4
3. Basic Physics of Magnetisation Transfer	5
3.1 Compartments of Magnetisation in Human Brain Tissue	5
3.2 Magnetisation Transfer	6
3.3 Magnetisation Transfer in Brain Tissue	12
3.4 MT Saturation Techniques	13
3.5 Applications of MT in MRI	15
3.6 A Dynamic Model for Pulsed MT	16
4. The STEAM Sequence	23
5. Absolute Quantification of the Proton MRS signal	24
6. Materials and Methods	25
6.1 The System and Sequence	25
6.2 Choice of the RF Saturation Pulse	26
6.3 System Restrictions	28
6.4 Agar Phantom studies	29
6.5 Patients and MT Protocol	29
6.5.1 Measurements of MT-dynamics	30
6.5.2 MT-Relaxometry Measurements	31
6.5.3 Analysis of MT-dynamics and Relaxometry data	31
7. Results and Discussion	32
8. Conclusion	46
9. APPENDIX A : EPIC Code of the MT Preparation Sequence	47
10. List of Abbreviations	55
11. Acknowledgements	55
12. References	56

1. Abstract

Magnetisation Transfer(MT) is a contrast mechanism in Magnetic Resonance Tomography (MRT). The technique uses the interaction between the invisible magnetisation in semisolid macromolecules(H_f) ($T_2 \ll 1\text{ms}$) and the water(H_f). After selectively saturation of the bound magnetisation H_f MT lead to a reduction of the water signal. The percentage loss of signal is expressed as MTR. A description of pulsed MT is of great importance in understanding the physical nature of the water signal from biological tissues and would establish a theory for an optimal MT sequence design.

Purpose

- i) To quantitatively evaluate Magnetisation Transfer(MT) in human brain. And to better understand the dynamics and give a description of the time dependency of MT for fast pulsed saturation.
- ii) To compare the effectiveness between the pulsed MT experiment and the continuous wave(cw) case and to study the MT-effect dependency for arbitrary saturation.

Material and Methods

Parietal white and grey matter in healthy volunteers were examined in a 1.5 T GE Signa MR scanner with the standard head coil. After presaturation of the bound pool H_f the water signal was detected by a localised STEAM sequence. The saturation was achieved by a chain of equidistant off resonance rf-pulses for various flipangles, offsets and time delay(TD) between the pulses. The approach to dynamic steady state was studied and analysed for different TD(15-100ms) and flipangles varying between 1080° - 1490° . Using a two pool model with linear exchange kinetics for magnetisation transfer and a simplified model for fast pulsed saturation, experimental data is possible to give the time dependence of the longitudinal magnetisation T_1 and exchange rate k_f of the semisolid pool for an arbitrary pulsed radiofrequency(rf) irradiation.

Results and Discussion

The MTR_{cw} was obtained from a linear fit of MTR^{-1} over TD for white matter as $87.7 \pm 2.3\%$ and $82.5 \pm 2.0\%$ for grey matter after correction for CSF partial volume($r > 0.993$). Within experimental accuracy the MTR_{cw} was independent of the arbitrary saturation left after one pulse and might therefore be used to compare MT effects of tissue quantitatively even for different saturation paradigms, including different scanners. For longer TD the steady state takes longer time to achieve. Curve fits of simplified derived expressions of pulsed MT gave $T_{1af} = 209 \pm 17\text{ms}$, $T_{1f} = 1620 \pm 170\text{ms}$ and $k_f = 4.2 \pm 0.4\text{s}^{-1}$ and for grey matter $T_{1af} = 248 \pm 17\text{ms}$, $T_{1f} = 1430 \pm 200\text{ms}$ and $k_f = 3.3 \pm 0.2\text{s}^{-1}$.

Conclusion

Using a conventional scanner and pulsed saturation we demonstrated that for short TD it is possible to derive the MTR_{cw} and to determine the kinetic constants for the free water using a two pool model of magnetisation transfer. The highest MTR was obtained for short TD and seemed strongly dependent on the TD. Through improvements and further investigations of the experiments a complete determination of the MT process *in vivo* might become possible.

2. Introduction

In MRI there are several more ways to create specific tissue contrast than the common T_1 or T_2 weighted SE experiments. A relatively new contrast mechanism is Magnetisation Transfer (MT), which is the subject of this work. In several clinical applications MT has improved MR Imaging (MRI) contrast: white matter diseases, breast imaging and musculoskeletal disorders(14).

Spin lattice relaxation (T_1) in tissue depends on several relaxation mechanisms, and hence on the biochemical composition and biophysical structure of the tissue. The predominant relaxation process involves magnetic dipole-dipole interaction of the nuclear magnetic moments, also referred to cross-relaxation, which is described as exchange of magnetisation between the involved nuclei. This exchange or transfer of magnetisation is the fundamental process of MT contrast.

For the sake of simplicity protons in biological tissue are assumed to exist in two pools: the "free" and the semisolid pool. The free pool or H_f -pool consists of mobile protons and has relatively long T_2 relaxation time, such those in water. The semisolid pool(also referred as the restricted pool) H_r consists of protons attached to macromolecules and has restricted mobility. Macromolecules are larger molecules like lipids or proteins. The signal of H_r can not be detected in ordinary MR experiments because of its extremely short T_2 time ($\ll 1$ ms).

At equilibrium the rates of loss and gain of magnetisation M_f are equal. However, the application of an off resonance radiofrequency(rf)-pulse will perturb the magnetisation of the semisolid pool and a new equilibrium will be build up by relaxation processes. The grade of perturbation or saturation is dependent on duration and frequency of the rf-pulse. After selectively saturation of the semisolid pool with an off-resonance rf-pulse, with narrow bandwidth, the detected signal will decrease. Ideally, the magnetisation of the H_f -pool is not directly affected by the pulse but only through cross relaxation processes. Saturation of the H_r is transferred to H_f , so the signal emitted by the H_f decreases. The relative decrease is called MT ratio and the amount of saturation transferred depends on the size of the H_r -pool, rf-pulse and interaction process.

There are two main approaches for MT saturation: continuous-wave (cw) and the use of pulses. In cw saturation, an rf field of singular frequency several kHz off resonance from water frequency is applied. However, this technique can not be applied on a conventional MR

scanner. Therefore, in clinical MRI high intensity rf-pulses have to be used. In contrast to cw, the dynamics of MT in a pulsed saturation experiment is not yet fully understood. There have been several different experimental saturation paradigms published for generating pulsed saturation. It also remains unclear which of these techniques gives the "best" contrast.

We present a theoretical and experimental description of fast pulsed MT which allows calculation of the kinetic constants of the free water pool *in vivo* and a derivation of the MTR for cw saturation. These calculations have before only been possible to obtain by use of the cw saturation technique.

The goal of this study is to understand the dynamics of pulsed MT. For this purpose a simple model of pulsed magnetisation transfer has been developed (see chapt. 3.5), which gives a quantitative description of the dynamic of MTR for different experimental parameters.

In order to study the dynamics of pulsed MT experimentally, we used a STEAM localisation in order to readout the water signal after an arbitrary number of rf-pulses. The acquisition was preceded by a equidistant chain of off resonance pulses. The method has the advantage that the parameters of the saturation may easily be changed (such as offset frequency, flipangle, time delay TD between the RF-saturation pulses) and the approach to steady state becomes observable.

The frequency and power dependence for MT were studied in agar phantoms. After establishing an experimental protocol studies were performed in grey and white matter of healthy volunteers. In the *in vivo* studies we varied TD and the flipangle of the rf-pulses to test our theory.

The aim of our MT studies is not to elucidate the various components of the more "realistic" model and their exchange rates, but rather get an insight into the dynamics to better understand MT in tissues. For that purpose a simplified model is sufficient and may be used to optimise MT methods for various clinical applications.

3. Basic physics of Magnetisation Transfer

3.1 Compartments of Magnetisation in Human Brain Tissue

Biological tissue is a complicated source of magnetisation. Cells, vessels, ventricles and extracellular space are different compartments, in which the water is contained. By definition

compartments are physically separated from each other. Compartments can be discriminated on the basis of different T_2 values of water. The compartmentation model of human brain tissue applied by Ernst, contains compartments of cerebral spinal fluid (CSF), structural material, and brain tissue (15).

The pure water content of CSF is normally 97 % and has T_2 relaxation times of approximately 1-2 seconds. Therefore CSF is almost completely visible in NMR. The structural material loosely corresponds to the macromolecules and water of very short relaxation time (McKay). The water content of tissue is less than for CSF and the macromolecule content is much larger and some of the signal corresponding to brain tissue will not be detected. The water in brain tissue has T_2 -times of about 60-400ms. By using an external standard the signal strength, which an identical volume of pure water would deliver, can be calculated and compared with the measured signal. By absolute quantification and iterative non least square fits of the T_2 relaxation , the CSF volume and the invisible "compartment" can be quantified.

Water, however, is not the only source of magnetisation. Protons are abundant in metabolites and macromolecules such as lipids and proteins. Relaxation times of metabolites depend on the molecular size and the medium. *In vivo* they therefore depend on the organ and compartment they are found in. In general the T_2 relaxation rates are on the order of 100-600ms (at 1.5T) for the metabolites and for the macromolecules \ll 1ms.

A T_2 -relaxation measurement in brain tissue is described by two singular exponentials, one with a T_2 relaxation time between 60-400ms and one >1000 ms, allowing estimation of the volume fraction containing CSF and the fraction of brain tissue. Extracellular water (EC) can normally not be detected because of similar relaxation rates in grey matter and low extracellular water content. In white matter pathologies however, a third compartment can be seen and detected as EC, see fig. 3.1.

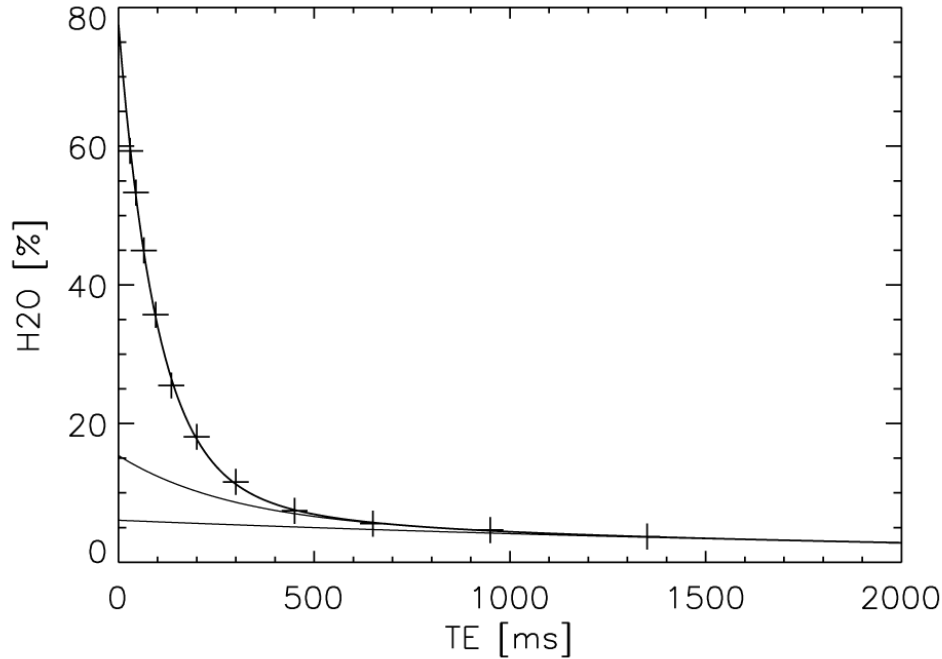


Figure 3.1 A T_2 relaxation measurement from an MS lesion. The three compartments of water are assigned to CSF, intra- and extra-cellular water.

3.2 Magnetisation Transfer Saturation (MTS)

Magnetisation of different kind (e.g. different molecules), shall be dubbed a “pool”. In magnetisation transfer saturation studies (also referred as magnetisation transfer (MT) studies) a two pool model is used. In other words the protons can by simplicity be assumed to exist in two pools: the “free” and the restricted pool. This simplification will further be discussed in chapter 3.3. The free pool, also referred as the H_f -pool, consists of relatively freely rotating water molecules. Protons of restricted mobility, i.e. those attached to macromolecules or water molecules in the surface layer of the macromolecules, are defined to exist in the semisolid pool H_r . These protons are not directly detectable in MR images, but the magnetisation of the restricted pool is present in its equilibrium state and may show interactions with the free water.

Generally, protons exist in number of compartments and pools. In relaxometry studies the compartments of water are estimated while in magnetisation transfer studies the interaction between the pools is especially of interest. The free pool of protons H_f or “free water” is the source of the NMR signal detected in common MRI. The restricted H_r -pool has an extremely short T_2 ($\ll 1$ ms), which makes it impossible to detect the signal directly.

Signal emitted by molecules in tissue have a characteristic absorption line shape. The H_f - pool has a Lorentzian line shape and the H_r -pool shows superLorentzian or Gaussian absorption behaviour (9,10). The area of the absorption line depends on the concentration of spins. The line width of a Lorentzian line shape at half height is $1/\pi T_2$. The line width of H_f is narrow due to its relatively long T_2 relaxation time. The corresponding line width of the restricted pool H_r is very broad - typically of the order 20 to 40 kHz. The broad spectral “peak” of H_r is assumed to be symmetrically located around the narrow frequency peak of H_f , see figure 3.2.

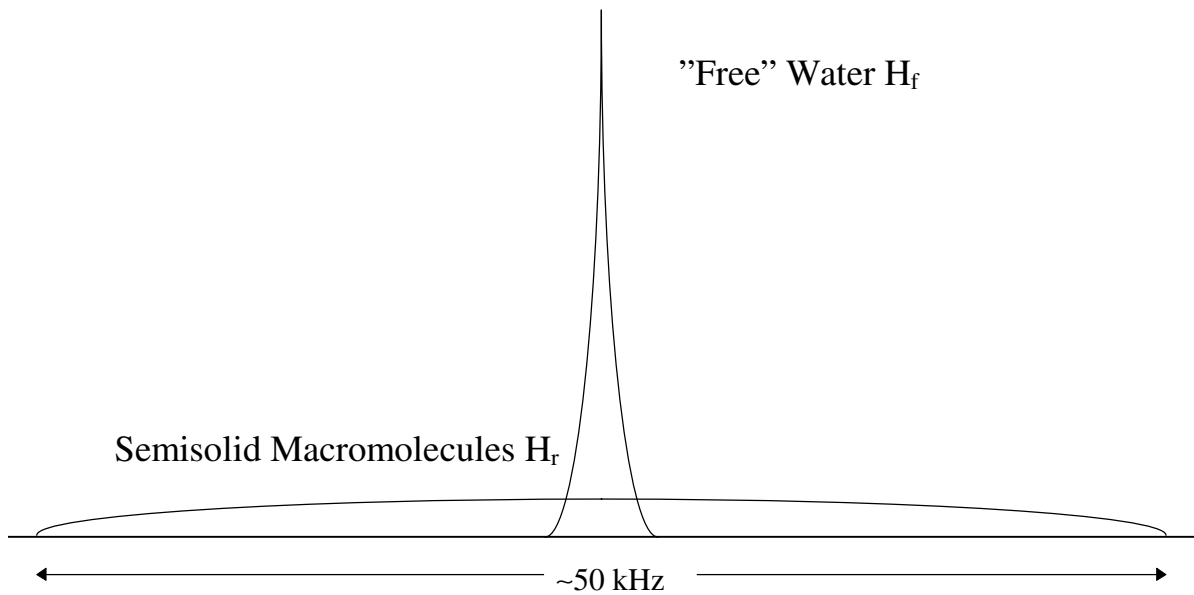


Figure 3.2 A schematic proton NMR spectrum of biologic tissue: resonance lines for the pool of mobile protons H_f (narrow peak) and the protons with restricted mobility H_r (broad peak). The line width is associated to the T_2 -time as $1/\pi T_2$. The two pools of protons interact with each other via cross-relaxation and chemical exchange.

The nuclear spin relaxation of water in biological tissues involves a number mechanisms and pathways. However, the predominant pathway of spin-lattice relaxation (T_1) in biological tissues has been shown to be the magnetisation transfer between the H_f - and the H_r -pool (4,6,7). In tissue the magnetisation transfer between macromolecular protons and water protons occurs mainly via dipolar cross-relaxation. Dipolar coupling between the nuclei makes it possible for magnetisation of the pools to be exchanged by cross relaxation processes. In some extent the MT effect takes also place via chemical exchange between the macromolecules and the surface layer of water which in turn communicates with the free water pool H_f . Figure 3.3 shows a schematic diagram of the possible interaction processes described above.

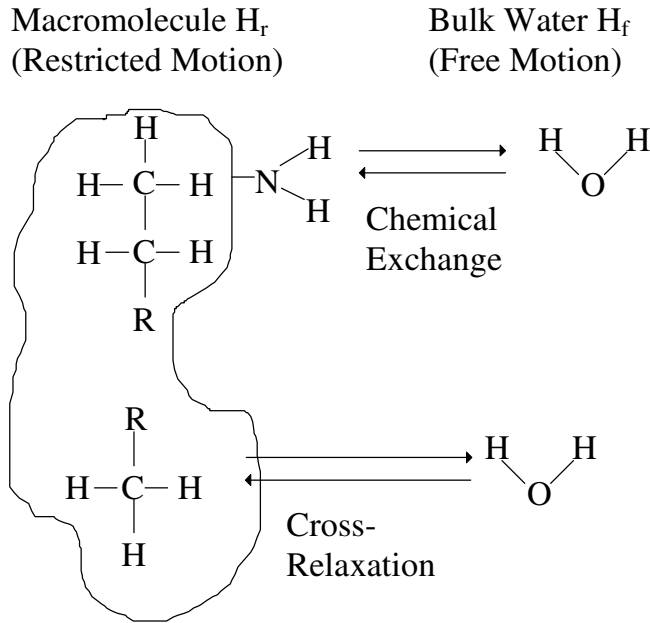
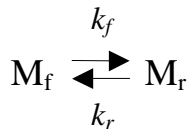


Figure 3.3 A Schematic diagram of water proton magnetisation transfer in biological tissues. In the cross-relaxation process the states of nuclear magnetisation are exchanged via dipolar coupling. The MT effect takes also place via chemical exchange, but cross-relaxation is the main pathway of the magnetisation transferred.

The simplest model to describe the magnetisation exchange is:



where M_r and M_f is the magnetisation of the H_r and H_f -pool and k_r and k_f its pseudo-first-order rate constants of magnetisation transfer between the pools. The exchange rates of magnetisation between each pool can be described by

$$\frac{dM_f}{dt} = -k_f \cdot M_f + k_r \cdot M_r$$

In equilibrium the transfer rates of magnetisation are the same:

$$\frac{k_r}{k_f} \equiv \frac{M_f}{M_r} \quad \text{eq.(3.1)}$$

The application of an rf-pulse will saturate the magnetisation of the H_r -pool and the equilibrium will be restored by the relaxation processes. The act of this saturation reduces the

population difference of the H_r -spins in the available energy levels. In other words if the H_r -pool is being selectively saturated no magnetisation is transferred from the H_r to H_f . However, magnetisation is still transferred from H_f to H_r , which is detected as a decrease in the intensity of the signal emitted by the H_r -pool. Because the signal decrease of H_f is caused by k_f , considering the equality in eq. (3.1), the MT rate will be the greater the larger H_r -pool.

The magnetisation experiment is schematically shown in fig. 3.4. The most used method to selectively saturate the semisolid H_r -pool is by applying an rf-pulse with a frequency deviating from the water frequency, i.e. an offset frequency. This decrease depends of the interaction processes (e.g. cross relaxation rates), the size of the H_r -pool and k_f . Consequently the MT-effect is tissue dependent: Tissues with high abundance of proteins will experience a greater loss of signal than a tissue with less, see fig. 3.5.

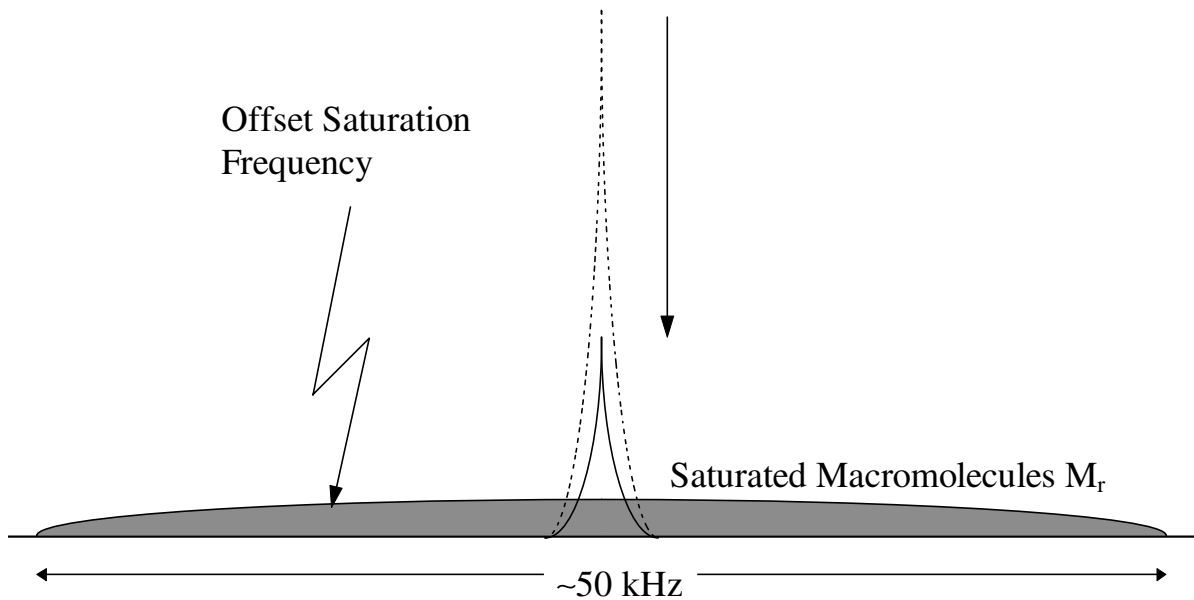


Figure 3.4 The Magnetisation Transfer Experiment

The protons of H_r is selectively saturated by an offresonance irradiation 1-5 kHz from the H_r resonance frequency while the free water pool hardly is affected. Magnetisation is transferred from H_r resulting in a signal decrease. The loss of signal depends on the exchange rate between H_r and H_f , amplitude, duration and offset frequency of the saturation pulse.

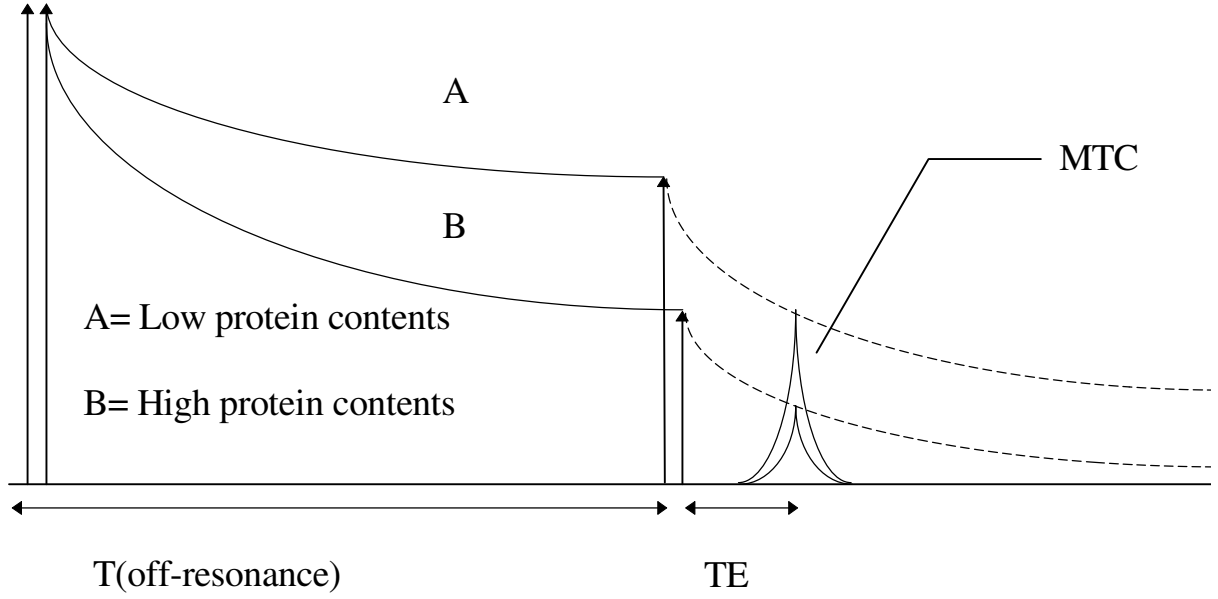


Figure 3.5 Applying off-resonance irradiation, tissues with high protein content will experience a higher degree of magnetisation transfer effect than tissue with higher water contents generating MTC between the tissues. The MTC is defined as $M_A^{MT} - M_B^{MT}$.

Signal loss is expressed as the difference between magnetisation without (M_0) and with (M_s) saturation divided by M_0 , see eq. 3.1. This relative signal loss is called MT ratio.

$$MTR = \frac{M_0 - M_s}{M_0} = 1 - \frac{M_s}{M_0} \quad (\text{eq 3.2})$$

A change in the observed T_1 relaxation time of the H_f -pool ($T_{1,f}$) is also caused by the magnetisation transfer saturation (6,11). The new relaxation time $T_{1,fsat}$ of H_f , which is shorter, and the magnitude of the H_f signal decrease are related to the rate constant k_f by following equation:

$$k_f = \frac{1}{T_{1,fsat}} \left(1 - \frac{M_{s,f}}{M_{0,f}} \right) \quad (\text{eq 3.3})$$

which only holds for full saturation of M_f after continuous wave irradiation (6). Provided that only the H_f -pool is saturated, i.e. no direct saturation of H_f MTR can be expressed as

$$MTR = k_f T_{1,fsat}$$

3.3 Magnetisation Transfer in Brain Tissue

Several models of different distributions of the H_1 -pool have been discussed in the literature (13,16) as a description of a true biological tissue system. A realistic model of the pools of water is of great interest for an understanding of the nature of the proton signal and its physical properties. The heterogeneity of tissue makes the model hard to determine. One realistic model assumes that water in biological systems consists of at least two free water pools and a multi pool system of macromolecules (16). In this model the magnetisation transfer becomes very complex, by multiple exchange pathways and pools. Concerning MT experiments, where the MT saturation affects the spins of different pools differently, parameters describing the MT exchange of the above model are almost impossible to determine. To characterise a model for MT studies further approximations have to be made.

A system represented by three or two pools is a well-recommended simplification to describe the tissue in vivo (16). In this simplified model of MT and pools of water following assumptions are made:

- i) The major relaxation component of the free water pool is dominant and minor components can be ignored.
- ii) For the case of two pools, the water bound to macromolecules (bound water) exchanges sufficiently rapidly with free water that free and bound water can be considered as a single pool.
- iii) Individual rates of transfer to the many macromolecular types can be represented by an average rate, i.e. an average single pool of macromolecules is only to be considered.

The aim of our MT studies is not to elucidate the various components of MT in a more realistic model and their exchange rates, but rather to get an insight into the dynamics of MT in tissues. For that purpose a simplified model is sufficient and the result may yield a model for optimising MT methods for various clinical applications. For our purposes brain tissue is supposed to consist in only two pools.

The detected signal comes from the compartments of cerebral spinal fluid (CSF) and brain tissue. The NMR-invisible compartment can roughly be identified with the structural material or dry weight of the brain and myelin water of $T_2 \approx 15\text{ms}$, and can be assessed quantitatively by comparing the signal strength of an external reference and the VOI, this will be discussed in chapter 5. The exchange rate between the mentioned pools and their individual relaxation

rates can be analysed by magnetic transfer experiments. Figure 3.6 shows a schematic model of the described pools and compartments of water in brain tissue. The CSF compartment consists mainly of free magnetisation, due to a very small content of macromolecules and is therefore assumed to be 100% visible. The literature tells that CSF does not show any measurable MT effect.

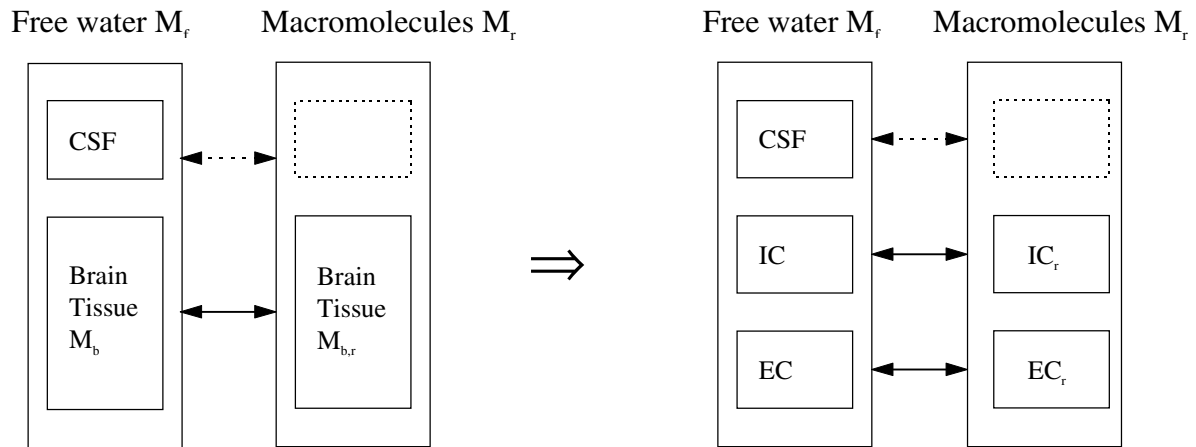


Figure 3.6 A schematic model of MT in brain tissue. The figure is an attempt to show the simplified model of interaction between different pools of magnetisation, split up in their compartments respectively. Ideally CSF does not contain any macromolecules therefore no MT effect should be present(dotted arrow). In pathological studies the right model should be used to better correlate with expected conditions.

3.4 MT Saturation techniques

There are two main ways to saturate the restricted pool: continuous wave (cw) and pulsed saturation. Continuous wave saturation is a long off resonance irradiation pulse with constant amplitude. When applying cw you usually reach steady state of the bound pool, but cw can not be applied on a conventional MR scanner and may be harmful for the subject because of high SAR values. It is therefore necessary to use the pulsed saturation technique in clinical MRI studies.

The pulsed saturation can either be done with an off-resonance pulse, i.e. a frequency deviating from the H_f -pool with narrow bandwidth, or by hard on-resonance pulses. The grade of saturation is dependent on duration, amplitude and frequency offset of the rf-pulse. Correspondingly the MT saturation is not only tissue dependent but also power and frequency dependent (4,11). By optimising the rf parameters the efficiency of the saturation can be

optimised. Ideally, the magnetisation of the H_f -pool is not directly affected. To avoid any bleed-over effect, the offset must be much greater than the bandwidth of the rf-pulse (normally $>700\text{Hz}$).

In the pulsed saturation case, a train of Gaussian or binomial pulses with short duration are applied before signal acquisition. For application of cw or Gaussian pulses, an off-resonance frequency gives a preferable saturation of the semisolid pool, because the absorption line shape of this pool is much broader than the liquid pool, see figure 3.6.

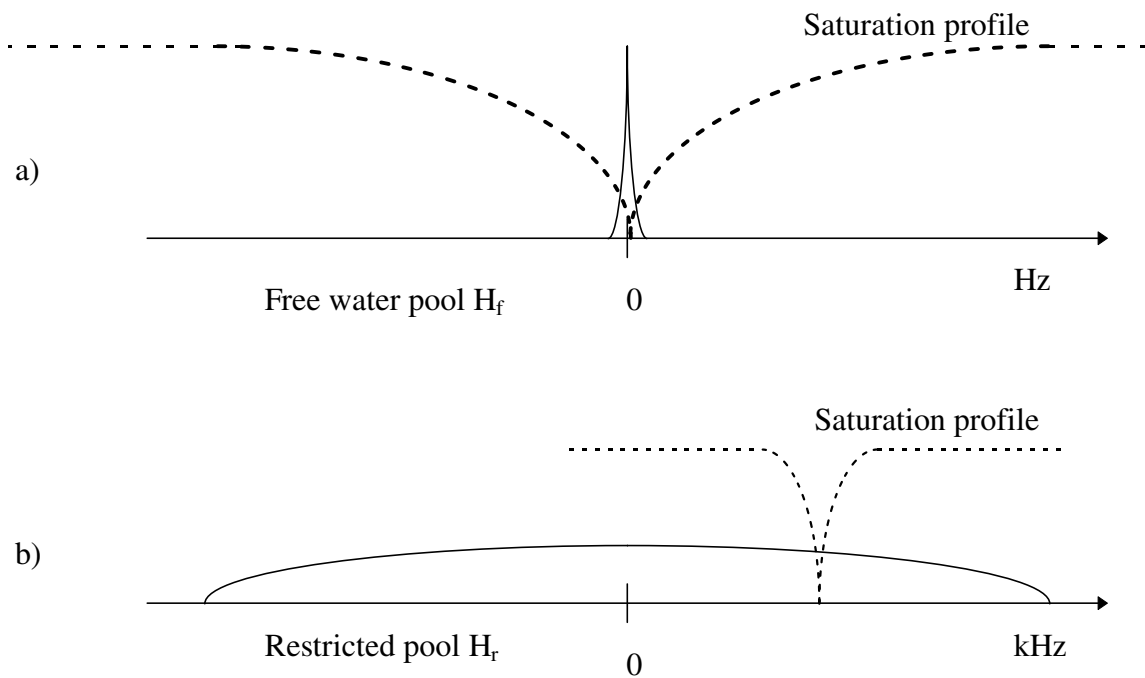


Figure 3.6 The saturation effect of a saturation pulse profile (dashed) on a) the H_f -pool and b) the H_r -pool. The figures is not to scale, therefore the saturation profile of water looks different in a) and b).

The pulse shapes of respectively technique are shown in figure 3.7. Width-modulated binomial pulses with varying polarity are typically applied on-resonance, such that magnetisation of the liquid pool receives a net flip angle 0° (ideally) while the semisolid pool is saturated. The T_2 relaxation time for the liquid pool is assumed to be sufficiently long for not losing any transversal magnetisation during the binomial pulses. As a result, when the area of the applied rf-pulses, with opposite polarity, equals the liquid pool receives a net flip angle 0° . On the other hand, the very short T_2 relaxation time for the semisolid pool ensures that all the transverse magnetisation of this pool is relaxing during the binomial pulse

increments, with the result that the longitudinal magnetisation in the semisolid pool becomes partially saturated. Although cw can generate higher contrast than binomial pulses, considerations of pulse duration favour binomial pulses, which makes them suitable in MRI. The binomial pulses on resonance are more power efficient than off resonance pulses, but because of their limited power ($A^2 \cdot pw$) they can not achieve as much MT effect as off resonance techniques.

In standard MT experiments the pulse duration of cw saturation is normally 3-5 seconds while the pulse duration of Gaussian pulses lies in the order of tenths of milliseconds and the binomial pulses are even shorter ($<2ms$), see figure 3.7.

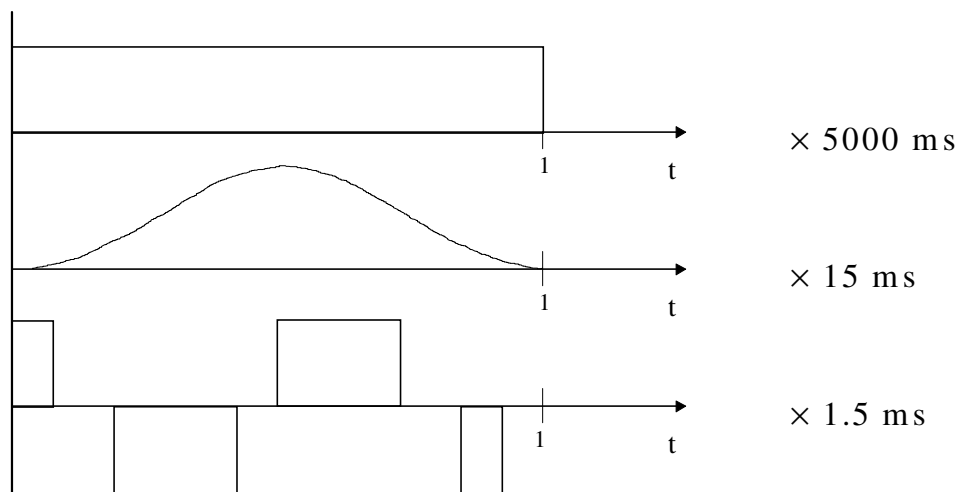


Figure 3.7 Representative RF waveforms used in MT saturation experiments. (a) CW rectangular pulse (b) Gaussian pulse and (c) a $\overline{1331}$ binomial pulse.

3.6 Applications of MT in MRI

In MR imaging other processes than different T_1 or T_2 times can be of interest. An MT experiment can provide information that is more tissue specific than obtained in ordinary imaging. The MT effect depends on surface chemistry and biophysical dynamics as well as concentration of macromolecules. A well defined MT saturation technique could result in a quantitative MT Imaging method, in which the spatial distribution of the MT process is shown.

In other words the result would yield quantitative pseudo-first-order rate constant (k_f), MTR- and $T_{1,f}$ -maps. Rate constant maps should prove useful in the quantitative characterisation of

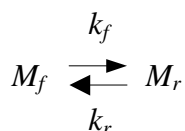
tissue relaxation processes and the improvement of tissue contrast in MRI (4). According to other authors this tissue characterisation is a promising method in diagnosis and characterisation of cancer, oedema, white matter diseases like multiple sclerosis (MS) or other pathologies, where the specific relaxation mechanism may be useful in determining the nature of the disease (4,14).

Another category uses MT as a tissue suppression technique, by which the contrast to adjacent structures is enhanced, e.g. MR angiography. White and grey matter and muscles show strong MT while blood does not. The enhancement of the contrast between the vessels and the adjacent tissue is a combination of the inflow effect of fresh spins of blood water and the fact that blood has a lower rate of MT. These facts will contribute to a much less H_r saturation of the blood than the adjacent static tissue. By more suppression of signal from tissue than blood the conspicuousness of blood vessels will be greatly improved. A schematic diagram illustrates the MT contrast between two tissues with different water/macromolecule interaction, see figure 3.4 in chapter 3.2. Generally MT contrast (MTC) enhances visualisation of lesions with increased water content, such in the neurological disease MS and different types of cysts with poor protein content. MT is also clinically valuable by the fact that gadolinium enhancement is magnified, resulting in lowering the dose of gadolinium as effectively as by a third (14).

For fast imaging techniques as gradient echo imaging, maximum MT signal difference occurs at excitation pulse angles below the liquid pool's Ernst angle ($\cos^{-1}[e^{-TR/T1,f}]$). Maximum MT signal difference for a binomial on resonance pulse and TR/TE of 50/7 ms occurred at approximately 16° and 13° for white and grey matter respectively, compared with Ernst angles in the absence of saturation of 21° and 16° , (13). Similar results are expected if off resonance pulses are used.

3.6 A Dynamic Model for Pulsed MT

The most simplified model for MT in tissue assumes a first order kinetic between the two pools H_r and H_f .



The assumptions have been discussed in chapter 3.3. In the case of absence of an rf field the longitudinal magnetisation M_f , M_r of the pools H_r and H_f is described by the Solomon equations

$$\frac{dM_f}{dt} = \frac{M_f^0 - M_f}{T_{1,f}} - M_f \cdot k_f + M_r \cdot k_r \quad \text{eq. (3.4)}$$

$$\frac{dM_r}{dt} = \frac{M_r^0 - M_r}{T_{1,r}} - M_r \cdot k_r + M_f \cdot k_f \quad \text{eq. (3.5)}$$

where M_r^0 and M_f^0 is the equilibrium z magnetisation, $T_{1,r}$ and $T_{1,f}$ are the longitudinal relaxation times and k_f and k_r the pseudo first order rate constants.

Using the equilibrium condition stated as before

$$M_r^0 \cdot k_r = M_f^0 \cdot k_f \quad \text{eq. (3.6)}$$

the equations 3.4 and 3.5 can be rewritten as

$$\frac{dM_f}{dt} = +(M_r - M_r^0)k_r - \frac{(M_f - M_f^0)}{T_{af}} \quad \text{eq. (3.7)}$$

$$\frac{dM_r}{dt} = -\frac{(M_r - M_r^0)}{T_{ar}} + (M_f - M_f^0)k_f, \quad \text{eq. (3.8)}$$

where T_{ar} and T_{af} are the apparent time constants, which are defined as

$$T_{ar}^{-1} = T_{1,r}^{-1} + k_r \quad \text{eq. (3.9)}$$

$$T_{af}^{-1} = T_{1,f}^{-1} + k_f \quad \text{eq. (3.10)}$$

Consider the MT experiment where the irradiation saturates the magnetisation in the H_r pool completely, i.e. $M_r = 0$. Equation (3.7) can be further simplified, while eq.(3.8) will not be valid any longer. The time dependence of M_f / M_f^0 will then be given by solving eq.(3.7) resulting in the familiar equation for saturation transfer (4)

$$\frac{M_f}{M_f^0} = \frac{T_{af}}{T_{1,f}} + k_f T_{af} e^{-(t/T_{af})}. \quad \text{eq. (3.11)}$$

Even for partial saturation of the restricted pool ($M_r = \text{const.} > 0$) the approach to steady state is monoexponential with time constant T_{af}

$$\frac{M_f}{M_f^0} = \left(\frac{T_{af}}{T_{1,f}} + \frac{T_{af} k_r M_r}{M_f^0} \right) + \left(k_f T_{af} - \frac{T_{af} k_r M_r}{M_f^0} \right) e^{-(t/T_{af})} \quad \text{eq. (3.12)}$$

For the purely theoretical case of the inverse experiment, in which only the magnetisation of the H_f pool is saturated, these equations can be rewritten by exchanging the prefix “f” for “r”.

For the easiest general solution the Solomon equations are rewritten for

$$\eta_f = \frac{M_f - M_f^0}{M_f^0} = C_1 e^{-\lambda_1 t} + C_2 e^{-\lambda_2 t} \quad \text{eq. (3.13)}$$

$$\eta_r = \frac{M_r - M_r^0}{M_r^0} = D_1 e^{-\lambda_1 t} + D_2 e^{-\lambda_2 t} \quad \text{eq. (3.14)}$$

The rates λ_1 and λ_2 are determined from the characteristic equation as

$$\lambda_{1,2} = 1/2 \left(\frac{1}{T_{ar}} + \frac{1}{T_{af}} \right) \pm 1/2 \sqrt{\left(\frac{1}{T_{ar}} + \frac{1}{T_{af}} \right)^2 + 4k_f k_r} \quad \text{eq. (3.15)}$$

and the coefficients $C_{1,2}$ and $D_{1,2}$ are determined by the initial conditions and

$$D_1/C_1 = -\frac{1}{k_f} \frac{M_r^0}{M_f^0} \left(\lambda_1 - \frac{1}{T_{ar}} \right) \quad \text{eq. (3.16)}$$

$$D_2/C_2 = -\frac{1}{k_f} \frac{M_r^0}{M_f^0} \left(\lambda_2 - \frac{1}{T_{ar}} \right) \quad \text{eq. (3.17)}$$

This follows the notation of Forsén and Hoffman (1), who have applied this model to measure chemical exchange. Their results can be directly applied to describe the MT ratio, because $MTR = -\eta_f$ (cf. 3.13).

Pulsed saturation

A suitable dynamic model for pulsed magnetisation transfer has to consider that the magnetisation H_r can only be partially saturated with short rf pulses. The degree of saturation is dependent on pulse shape, rf power, offset frequency and on the *true* physical features of the semisolid pool and may not be predicted reliably. Quite contrary, in cw measurements the MT is used to study how the restricted magnetisation is saturated for different off resonance frequencies. During the repeated delay TD magnetisation tend to relax to its equilibrium state. We describe the saturation of H_r created by the pulse by the fraction of magnetisation, which

is left after one pulse $\alpha \cdot M_r$, and assume that α is independent of M_r , i.e. of the T_1 relaxation during the pulse. During the delay between until the next pulse the system will evolve to a new state according to the Solomon equations.

Following approximations, definitions and assumptions have been made in the model:

- Singular T_1 of the H_r -pool, i.e. H_r has a Lorentzian absorption behaviour.
- After the rf pulse a fraction α is left of M_r , which means that we neglect the influence of relaxation on the saturation. No direct saturation of the free water.
- The relaxation and MT during the rf pulse are accounted for by adding the pulse length to the time between the pulses. The time delay TD is defined as the time from the beginning of the n th pulse until the $(n+1)$ th pulse.

A schematic model of the pulsed MT experiment is shown in figure 3.8 below. The fractional saturation of the semisolid magnetisation is shown by α and the magnetisation M_r and M_f after the n th pulse and the delay is represented as the vector η^j . The remaining magnetisation of the free water is read out locally by a STEAM signal $S \propto M_f$

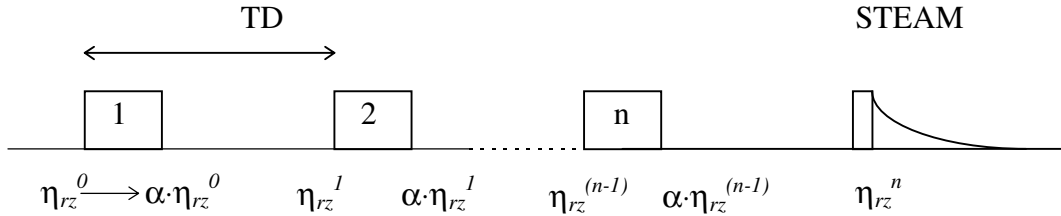


Figure 3.8 A schematic model of the pulsed MT experiment. The magnetisation is expressed as vector η^j , which is saturated by the instantaneous rf pulse and evolving during the repetition period TD according to the Solomon equations. α describes the fraction of magnetisation left after one saturation pulse and represents a saturation of H_r only. Relaxation between the pulses is accounted in the calculations, whereas relaxation during the saturation pulses is neglected. In the actual experiment, bell shaped single lobe pulses are used.

The evolution of η_f and η_r during the saturation pulse chain can be cast into a recursion for the vector η^j . The saturation of H_r takes the form

$$\begin{pmatrix} \eta_f \\ \eta_r \end{pmatrix}^{j+1} = \begin{pmatrix} 1 & 0 \\ 0 & \alpha \cdot \end{pmatrix} \begin{pmatrix} \eta_f \\ \eta_r \end{pmatrix}^j + \begin{pmatrix} 0 \\ \alpha - 1 \end{pmatrix} \quad \text{eq. (3.18)}$$

and the components are coupled by the free evolution during TD giving

$$\begin{pmatrix} \eta_f \\ \eta_f \end{pmatrix}^{j+1} = \begin{pmatrix} F & f \\ \alpha \cdot r & \alpha \cdot R \end{pmatrix} \begin{pmatrix} \eta_f \\ \eta_f \end{pmatrix}^j + \begin{pmatrix} 0 \\ \alpha - I \end{pmatrix}, \quad \text{eq. (3.19)}$$

where f , F , r and R are derived using eq. (3.15-17).

A matrix recursion of the form $\eta^{j+1} = A \cdot \eta^j + b$ gives

$$\eta^{j+1} = (E-A)^{-1} \cdot (E-A)^j \cdot b, \quad \text{eq. (3.20)}$$

where E is the unity matrix. After diagonalisation of A by the unitary matrix U

$$A = \begin{pmatrix} F & f \\ \alpha \cdot r & \alpha \cdot R \end{pmatrix} = U \cdot \begin{pmatrix} \mu_1 & 0 \\ 0 & \mu_2 \end{pmatrix} \cdot U^{-1} \quad \text{eq.(3.21)}$$

equation (3.21) takes the form

$$\eta^j = U \cdot \begin{pmatrix} \frac{1-\mu_1^j}{1-\mu_1} & 0 \\ 0 & \frac{1-\mu_2^j}{1-\mu_2} \end{pmatrix} \cdot U^{-1} \cdot \begin{pmatrix} 0 \\ \alpha - I \end{pmatrix}. \quad \text{eq. (3.22)}$$

μ_1 and μ_2 are the roots of the characteristic equation of A :

$$\mu_{1,2} = 1/2(F + \alpha \cdot R) \pm 1/2\sqrt{(F + \alpha \cdot R)^2 + 4\alpha \cdot f \cdot r} \quad \text{eq. (3.23)}$$

Because this equation governs also the components of U , the amplitudes of the two exponentials are coupled and the degrees of freedom is reduced to 3. The MTR observed at the free water signal after the n th pulse is

$$MTR(n) = -\eta_f = \frac{A}{(\mu_1 - \mu_2)} \left[\frac{1 - \mu_1^{n+1}}{(1 - \mu_1)} - \frac{1 - \mu_2^{n+1}}{(1 - \mu_2)} \right], \quad \text{eq. (3.24)}$$

where $A = (\alpha - I) \cdot f$. Letting the number of pulses n approach the limit of infinity

$$\lim_{n \rightarrow \infty} MTR(n) = \frac{A}{(\mu_1 - \mu_2)} \left[\frac{1}{(1 - \mu_1)} - \frac{1}{(1 - \mu_2)} \right]$$

we get the steady state value

$$MTR_{ss} = \frac{A}{(1 - \mu_1)(1 - \mu_2)}. \quad \text{eq. (3.25)}$$

Approximation for short pulse repetition periods

For short TD the components of A and hence the expressions for μ_1 , μ_2 and MTR_{ss} can be simplified considerably by linearisation under the assumption $TD \ll k_f^{-1}, k_r^{-1}, T_{af}, T_{ar}$:

$$\begin{aligned} F &= 1 - \frac{1}{T_{af}} TD \\ R &= 1 - \frac{1}{T_{ar}} TD \\ f &= k_f \cdot TD \\ r &= k_r \cdot TD \end{aligned} \quad \text{eq. (3.26)}$$

$$MTR_{ss}(TD) = k_f \cdot T_{laf} \cdot \frac{1}{(1 + B \cdot TD)}, \quad \text{eq. (3.27)}$$

where B is a constant depending on the kinetic parameters

$$B = \frac{\alpha}{1 - \alpha} \left(\frac{1}{T_{ar}} - k_r \cdot k_f \cdot T_{af} \right). \quad \text{eq. (3.28)}$$

Because the dependence on TD is simplified it becomes possible to derive constants like B from a fit of eq. 3.28. Together with similar expressions for μ_1 and μ_2 all kinetic parameters and the unknown saturation factor α can be derived. However, if $\alpha \ll 1$, μ_2 becomes linear in α and thus very small and may, therefore, not accurately be determined.

$$\mu_2 = \alpha \cdot R - \alpha \cdot \frac{f \cdot r}{F - \alpha \cdot R} \quad \text{eq. (3.29)}$$

In order to fit the dominating $\mu_1(TD)$ it has to be further simplified, which is possible by linearisation for $\alpha \ll 1$, i.e. high degrees of saturation:

$$\mu_1 = F + \alpha \cdot \frac{f \cdot r}{F - \alpha \cdot R} \quad \text{eq. (3.30)}$$

With this second approximation (3.23) finally takes the form

$$\mu_1(TD) = 1 - \frac{TD}{T_{laf}} \cdot \frac{\left[1 - \frac{TD}{T_{laf}} + B \cdot TD \right]}{\left[1 - \frac{TD}{T_{laf}} + C \cdot TD \right]}, \quad \text{eq. (3.31)}$$

with B as in eq. (3.29) and

$$C = \frac{\alpha}{1-\alpha} \cdot \frac{1}{T_{ar}} \quad . \quad \text{eq. (3.32)}$$

From the approach of M_f to steady state for different small values of TD it is possible to determine $\mu_l(\text{TD})$ and $MTR_{ss}(\text{TD})$. From the constants in eqs. (3.27) and (3.31) it possible calculate k_f , T_{laf} and $k_r \cdot T_{lar}$. α and the individual k_r and T_{lar} remain unknown, which makes it difficult to check, whether the assumptions have been met.

Extrapolation to Continuous Wave Saturation

The equation (3.27) makes it possible to compare pulsed and cw saturation. With $MTR_{cw} = k_f \cdot T_{laf}$ it can be rewritten

$$MTR_{ss} = MTR_{cw} \cdot \left[1 + \frac{D \cdot \alpha}{(1-\alpha)} TD \right]^{-1}, \quad \text{eq. (3.33)}$$

$$\text{with } D = \frac{1}{T_{ar}} - k_r \cdot k_f \cdot T_{laf}.$$

The full cw saturation is approached as a limes for both $\alpha \rightarrow 0$ and $TD \rightarrow 0$:

$$MTR_{cw} = \lim_{TD \rightarrow 0} MTR_{ss} = \lim_{\alpha \rightarrow 0} MTR_{ss} \quad \text{eq. (3.34)}$$

MTR_{cw} is reached in the hypothetical cases of extrapolation beyond the validity of the model: Complete saturation ($\alpha=0$) after one pulse implies a pulse length of the order of T_{ar} , i.e. the saturation can no longer be regarded as instantaneous. The pulse repetition delay TD cannot be decreased below the length of the saturation pulse. Nevertheless it is possible to derive MTR_{cw} from the saturation obtained at short TD. As MTR_{cw} is no longer dependent on the experimental parameters α and TD it offers a possibility to compare MT experiments despite different saturation paradigms or MR systems.

4. The STEAM sequence

STEAM (STimulated Echo Acquisition Mode) is a localisation technique based on a stimulated echo created by three slice selective 90° pulses. Provided with proper selection of the STE, the signal will result from the VOI formed by the intersection of the three slices, see figure 4.1. Other FIDs and echoes are dephased by crushers gradients between the pulses.

A great advantage of localised methods is that the homogeneity of the magnetic field can be locally optimised for the VOI by shimming the gradients. The localised methods, STEAM and PRESS are single shot techniques and the signal from the VOI is detected instantaneously. This makes the spectroscopy methods preferable for detecting MT on the way to steady state.

Compared to PRESS, which uses a double spin echo for localisation, shorter echotimes are possible with STEAM. STEAM is also less sensitive to pulse and gradient imperfections and the signal decreases less by T_2 relaxation, relatively the PRESS method, because the relevant magnetisation is stored as longitudinal magnetisation between the second and the third pulse. A disadvantage of the STEAM method though a signal loss of 50%, inherent to the stimulated echo method.

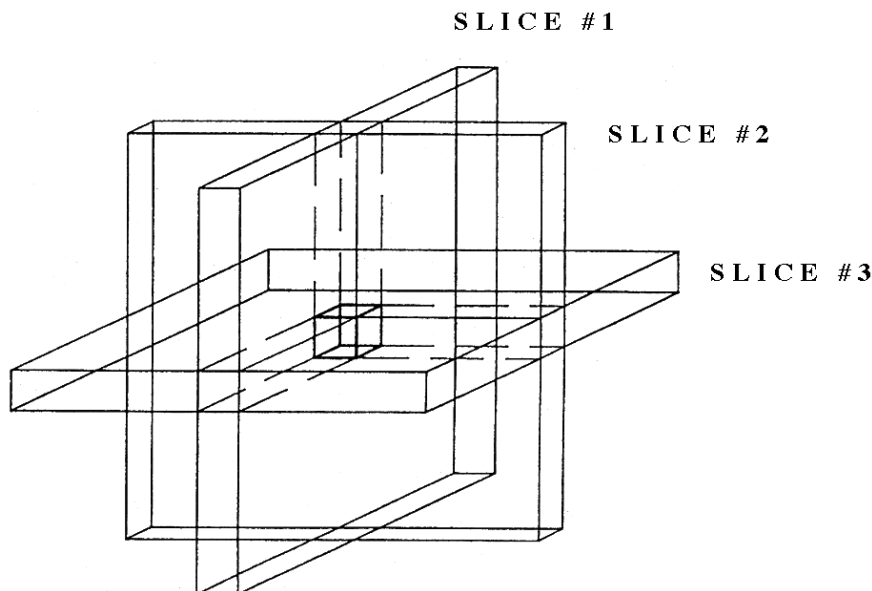


Figure 4.1 Three selected slices creating the Volume of Interest.

5. Absolute Quantification of the Proton MRS Signal

For an absolute quantification of the water signal, a correction of the sensitivity is necessary. This should be based on the water signal from an external reference and the local Transmitter Gain (TG) value. Quantification of the water contents in the tissue a comparison to another signal of which the concentration is known has to be done. Because changes of the

experimental conditions can not be avoided these have to be corrected for in order to achieve full comparability of the measured signal(17).

The local TG value is determined from a fit of 6 TG points, corresponding a maximum amplitude of the signal. In contribution with correction of the T_2 relaxation it is then possible to express the tissue water contents as the relative fraction of the calculated signal of 100% distilled pure water under the same physical conditions.

Determining $TG(x)_{true}$ we can get an expression of the actual flipangle $\theta(x)_{true}$.

$$\theta(x)_{true} = \frac{TG_{nom}}{TG(x)_{true}} \theta_{nom} \quad \text{eq.(5.1)}$$

where TG_{nom} is user specified and $TG(x)_{true}$ is a estimated true local TG value corresponding to maximum signal, i.e. an actual flipangle of 90° . $TG(x)_{true}$ is received from a fit of the theoretical signal dependence to different TG_{nom} values. This procedure is used to individually calibrate the flip angle for each VOI. Using the corrected external signal $S_{corr}^{ext} = S^{ext} \cdot TG(x)_{true}^{ext} / V^{ext}$, the corrected signal S_{corr} can be expressed as:

$$S_{corr} = S \cdot \frac{TG(x)_{true}}{V / S_{corr}^{ext}} \propto M_{tr} \quad \text{eq(5.2)}$$

All scanner specific dependencies of the sensitivity are removed by equation (5.2) and all the sequence and sample specific dependencies are contained in M_{tr} . The transversal magnetisation M_{tr} is in turn dependent on the localisation method and actual flipangles used, relaxation rates and timing parameters, the field strength and the temperature. Throughout this work we have used the STEAM localisation method for which the transversal magnetisation $M_{0,tr}$ (neglecting relaxation process) depends on the actual flipangle

$$M_{0,tr} = 1/2 M_0 \cdot \sin^3(90^\circ \cdot TG_{nom} / TG(x)_{true}) \quad \text{eq.(5.3)}$$

and with the relaxation effects included

$$M_{tr} = M_{0,tr} \cdot e^{-TE/T_2} \cdot [1 - e^{-TR/T_1}] \cdot e^{-TM/T_1} \quad \text{eq.(5.4)}$$

Equation 5.2-5.4 allow a complete quantification of the concentrations from the localised NMR signal.

6. Materials and Methods

6.1 The System and Sequence

All studies were performed on a 1.5 T GE Signa Advantage using the standard cp head coil (28 cm birdcage). For our measurements STEAM was chosen by preference over PRESS because it is well established at our system. For selective saturation of the H_r -spins a preparation sequence contained of a chain of equidistant single lobe rf pulses was developed by modifying the CHESS water suppression of the localised spectroscopy sequence. The sequence was programmed in EPIC, the GE pulse program language. In order to dephase the transversal magnetisation left after the partial saturation of H_r , magnetisation spoilers with low amplitude were located between the saturation pulses. The user is allowed to specify the distance between pulses (TD), number of rf pulses (n), frequency offset ($\Delta\nu$), flipangle (θ) and the pulse width (pw). After the time of saturation the water signal is detected in a single localised STEAM acquisition, see figure 6.1.

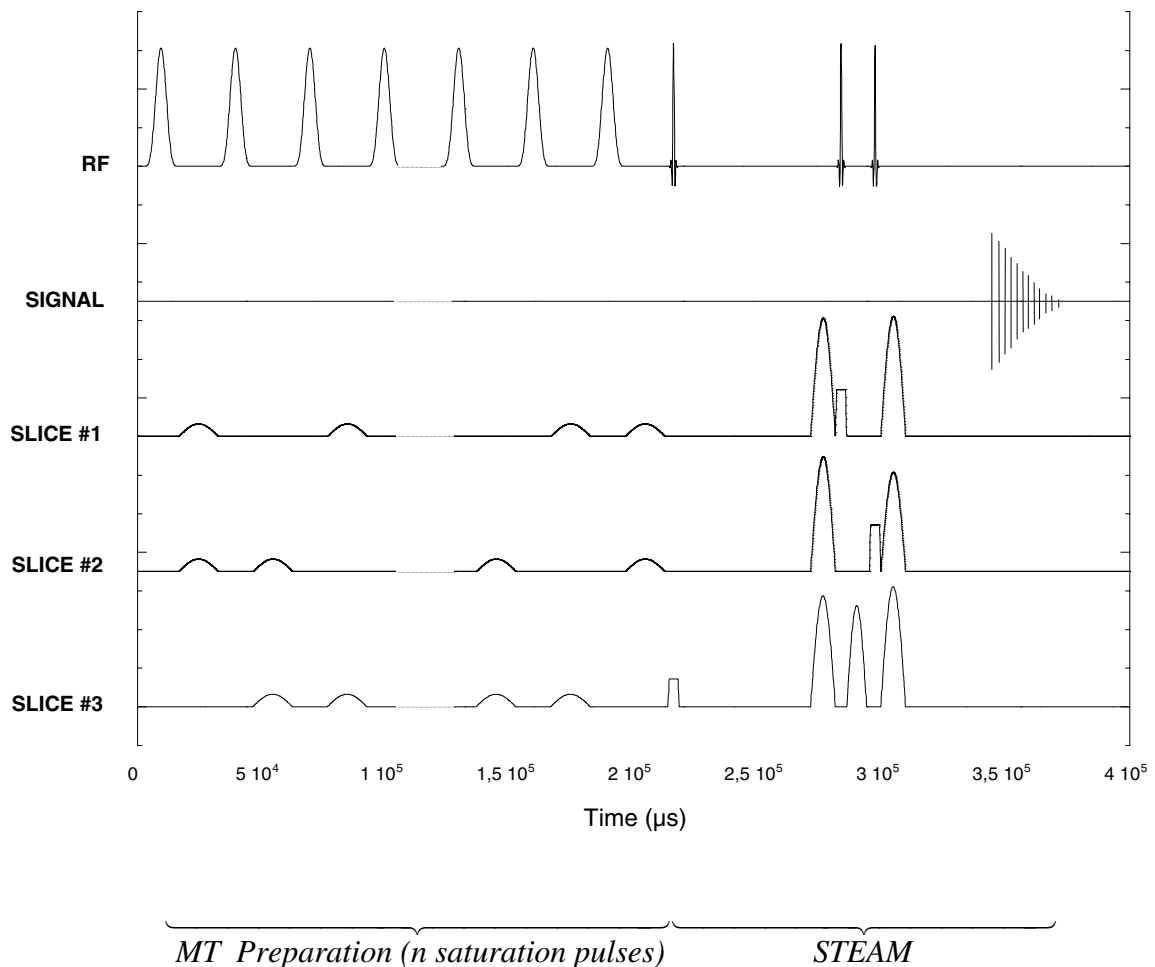


Figure 6.1 The STEAM sequence with MT preparation. The spoiler gradient scheme in the MT preparation chain is repeated each 3 pulses. The rectangles are the slice selective gradients. The refocusing is done during the sine bell shaped spoilers. These considerably reduce the induction of eddy currents.

6.2 Choice of the RF Saturation Pulse

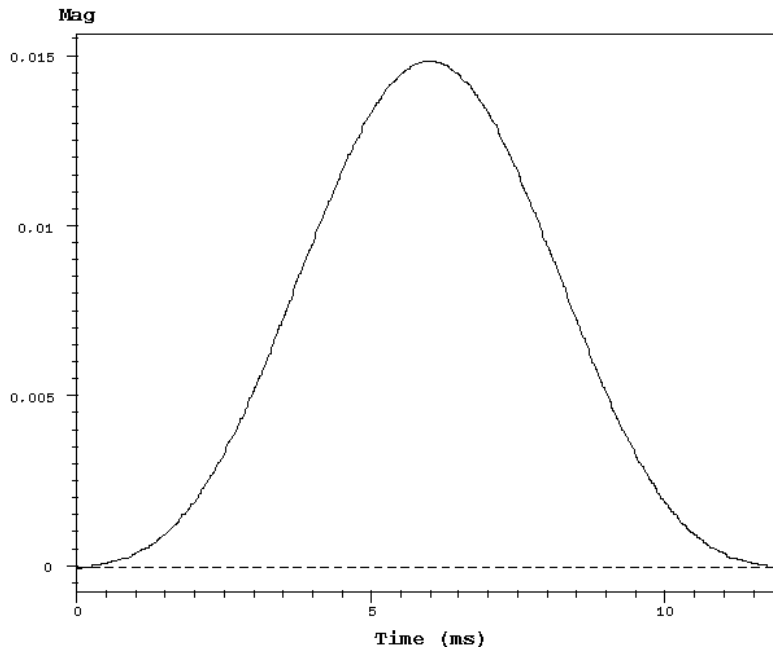
Because no Gaussian pulse shapes were available on our system, we choose another single lobe pulse for saturation. The mainlobe of a sinc pulse was multiplied with a hamming filter in order to smoothen the edges, see fig. 6.2.

Because of the power dependence of MT, short pulses with high amplitude expects to be more efficient than long pulses with lower amplitude. Furthermore, agar phantom studies showed that a more effective saturation is achieved with shorter TD, favouring the use of short pulses. In order to avoid direct saturation of the H_F -pool a narrow bandwidth and a sufficiently high offset is required. A higher bandwidth demands a higher offset and vice versa. The pulse width and the "minimum" offset frequency were set to 12ms and 1kHz. The bandwidth proved to be narrow enough avoiding direct saturation of the H_F -pool, see chapt.7. Table 6.1 shows the basic trade offs for choosing the pulse width.

The pulse is sampled in a finite number of timepoints. Therefore to avoid problems with offset frequencies affecting the free water frequency, the sampling interval Δt has to be selected so that the maximum offset $\Delta v < 1/(2\Delta x)$ (Nyquist theorem). Our pulse of 12 ms contains of 1000 timepoints, giving a maximum offset frequency of 42,6 kHz, which can be regarded sufficient for the H_F -pool not to be affected. The minimum sampling interval for the MR system is limited to 4 μs and therefore, the selected pulses must not be too short. If longer pulsewidths is wanted, more sample points have to be set.



MRCE/Rf

**Tech Report**

No. of time pts: 1000
 Flip angle(deg): 360.00
 Pulse Duration(ms): 12
 Maximum B1(G): 0.04637
 Energy(G**2 ms): 0.007918
 isoDelay(ms): 4.14
 FW 10% Max (kHz): 0.1590
 FW 50% Max (kHz): 0.8071
 FW 71% Max (kHz): 1.1474
 FW 90% Max (kHz): 1.4553

RF Heat {Head}

Inputs
 SAR(Kg): 74.00
 cfhpdl: 4000.000 cfhpsl: 1166.000
 cfhpsv: 2800.000 cfhpsc: 0.300
 cfhlrr: 1135.000 cfloss: 1.023
 rfupa: -250 rfupd: 050
 occal: 1.0000 ccjcoil: 0.3798
 Analysis
 MinTr: 3.551 DPlate: 35.505
 RFOut: 7.266 PwrSply: 42.771

Figure 6.2 The pulse shape of the saturation pulse and calculated SAR values.

Table 6.1 Trade Off's in choosing the pulse width of an off-resonance saturation pulse. To compare the pulses, the power of the pulses are assumed to be the same. The ! tells that we may have a problem here(worst case).

	Long Pulses	Short pulses
SAR ~1/pulsewidth	OK!	! SAR to high
Flipangle θ ~ pulse width	OK!	! θ not achieved
MTR ~ power $P \sim \int A_{max}^2 dt$! Less MT effect	OK!
Minseqrfamp(software)	! Software problem	OK!
Direct saturation (Bandwidth ~ 1/pulsewidth)	OK!	! The H_f affected

Short TD	!	OK!
Minimum sampling interval 4 μ s	OK!	!

6.3 System restrictions

System software and hardware gave us following limitations of the free choice of parameters.

- 1.) The system routine minseqrfamp restricts the total number(n) of pulses of given amplitude irrespective the time delay (TD) between the RF-pulses. This restriction appears somewhat unmotivated because the duty cycle of the RF-amplifier should cause problems only for narrow pulse spacing. For instance, for a pulse of 1440° a limitation of 40 saturation pulses is set.
- 2.) The length of the preparation sequence is limited to a maximum of 1.6 seconds, which is the most severe restriction for reaching steady state. For TD values greater than 50 ms a preparation of at least 2.5 seconds should be sufficient to reach steady state, see chapt. 7.

These limitations gave us severe problems reaching steady state. Possible improvement through better hardware should allow the preparation time to be longer and the RF-amplifier software should be changed to better fit the duty cycle of the RF-amplifier, resulting in a fully achieved steady state.

- 3.) The maximum allowed flipangle is dependent on the highest possible pulse amplitude coming from the RF-amplifier and the user specified pulse width ($\theta = \gamma \int B_1 dt$). For our settings a flipangle of 1500° was the maximum.
- 4.) Dependent on limits of SAR(Specific Absorption Rate) we also have a restrictions concerning total heat deposited in the patient. However the restrictions of 1.) and 2.) has always been larger, therefore SAR limits has never been a problem.
- 5.) Eddy currents. In some measurements the system show a fluctuation in the received signal, which we believed be due to eddy currents, which particularly is a problem for localised methods. These considerably have effects of the reproducibility.

6.4 Agar Phantom Studies

Studies in a 2% agar phantom were done to test the behaviour of the MT saturation and to optimise the paradigm for the *in vivo* studies. Three kinds of MT studies were done: measurements of the power, frequency and TD dependence. In order to prove the power dependence, the saturation for different pulsewidths and flipangles but with the same power integral was studied at different offsets. The frequency dependence was studied by measuring the signal after a constant time of saturation for different offset frequencies.

6.5 Patients and MT Protocol

This study was performed over a 2-month period and involved 14 healthy volunteers (aged 19 to 40 years). The volunteers were recruited from relatives or co-workers of the author and have been fully informed about the experiment before each examination.

At first a scout image in the central sagittal plane is done giving the coordinates for the reference phantom and to place the 3D box. Signal from the reference, using STEAM, was collected by 6 non suppressed scans for different TG values ranging between 40 and 115. A TG-fit of these data determined the TG of maximal signal, i.e. $TG(x)_{true}$, and the corrected external water signal S_{corr}^{ext} .

On a set of 3D FLASH images the VOI were placed in parietal grey and white matter in the healthy volunteers. Volume of interest was in the range of 4ml to 11ml. A manual shimming and adjustment of the water frequency was done for every VOI to improve the reliability of the signal. The water signal was measured by the STEAM acquisition prepared by the saturation sequence. For these measurements a TG value (TG_{nom}), as close to $TG(x)_{true}$ as possible, is used to ensure optimal reproducibility of the flipangle. By this TG measurements the flipangle can be adjusted within $\pm 1\%$ variation. This is especially important in the saturation experiments because of the varying water signal. For every new VOI the same procedure for measuring the local $TG(x)_{true}$ is made. Now we have all parameters to make an absolute quantification of the water signal received in the VOI. This is possible by using the equations described in chapt. 5.

Two kinds of experiments were made namely MT-dynamics and MT-Relaxometry, which are described in detail below. For the relaxometry protocol we used, in contrast to the dynamic measurements, constant values of the number of pulses n , flipangle, and TD.

6.5.1 Measurements of MT-dynamics

In this part of the work we wanted to study the dynamics of the MT effect to test the two-pool model, described in chapter 3.6. Our main purpose was to get a theoretical description of the $MTR_{ss}(TD)$ and time constants $\mu_1(TD)$ giving the values of the kinetic constants.

As mentioned in chapt. 3.3, CSF is assumed to show no MT effect, therefore the CSF contribution of the signal must be subtracted in the MT measurements. Due to the relative high CSF content in grey matter VOIs, relaxometry measurements were performed in order to correct for the CSF content for grey matter measurements. In white matter this correction was not needed because the VOIs were placed, so that they contained no CSF.

The number of saturation pulses n , flipangle and TD value were the main parameters that were varied during the dynamic studies. To prove the eq. 3.24 experimentally, the approach to steady state was determined, i.e. the MTR was measured dependent of number of pulses and fitted by eq. 3.24. In order to determine time and flipangle dependence of MTR_{ss} and $\mu_{1,2}$, these measurements were done for TD values ranging between 15 -100ms and for three different flipangles 1080° , 1240° and 1440° at 1kHz offset frequency.

The reference signal M_0 , i.e. magnetisation without MT saturation (MT_{off}), is a average signal of six or more equal STEAM acquisitions with MT-preparation and zero flipangle. This mean calculation is necessary due to system instability.

6.5.2 MT-Relaxometry Measurements

In the second part of this work we measured the T_2 -relaxation of the water signal in order to study signal changes due to MT of different compartments contained in the VOI. For different values of TE we sampled the magnetisation when relaxing in the transversal plane, giving a total estimation of the T_2 relaxation times for the compartments. The acquisition of the water signal for the VOI *in vivo* was done at 12 TE values logarithmically placed between 20ms and 2 s.

The main purpose of this study was to check whether CSF does show any MT effect or not.

6.6 Analysis of MT-dynamics and Relaxometry data

The observed relative signal after a train of n pulses can be fitted by MTR as eq. 3.24. After sufficient number of pulses the magnetisation will reach the dynamic steady state MTR_{ss} , i.e. when the signal is no longer changing with the number of pulses. The approach to steady state for different TD values was analysed by a Non Linear Least Square fit (NLLS), in Kaleida graph on a mac, to the estimated $MTR(n)$ values giving the values of MTR_{ss} and the time constants $\mu_{1,2}$ for a given TD. These were in turn fitted by the formulas derived from the theory for fast pulsed saturation, eq. 3.27 and 3.31.

The relaxometry data were analysed in a IDL program, on a Sun work station, using a two compartment model. Every tissue compartment has its own specific T_2 relaxation time (CSF~2500ms and IC~60-70ms). And by assuming that the tissue can be approximated by two compartments of water the program is estimating the best fitted relaxation curve for each pool using a NLLS fit. Relaxation times and relative tissue contents can be determined from the fit.

7. Results and Discussion

Phantom experiments

The initial task was to choose an appropriate saturation paradigm. A 2% agar phantom was used to test the MT preparation sequence. We found relative large differences between acquisitions without MT preparation and with MT but a flip angle of zero degree. No saturation should theoretically be expected in this case. This signal decrease can be explained to be dependent by direct saturation of the H_f -pool by noise leaking from the unblanked rf-transmitter. This should also take place during the MT saturation and, therefore the reference signal S_0 has to be obtained at zero flipangle. *In vivo* the direct saturation due to rf-leakage

was not as severe as in the phantom studies. In fact this effect was of the same order as the uncertainty in the measurements.

In figure 7.1 the offset dependence of the H_f saturation is shown for different pulsewidths and flipangles but with the same power integral. The greater flip angle and shorter pulse width, the better saturation, as seen in the figure. The effect was symmetrical in frequency (not shown).

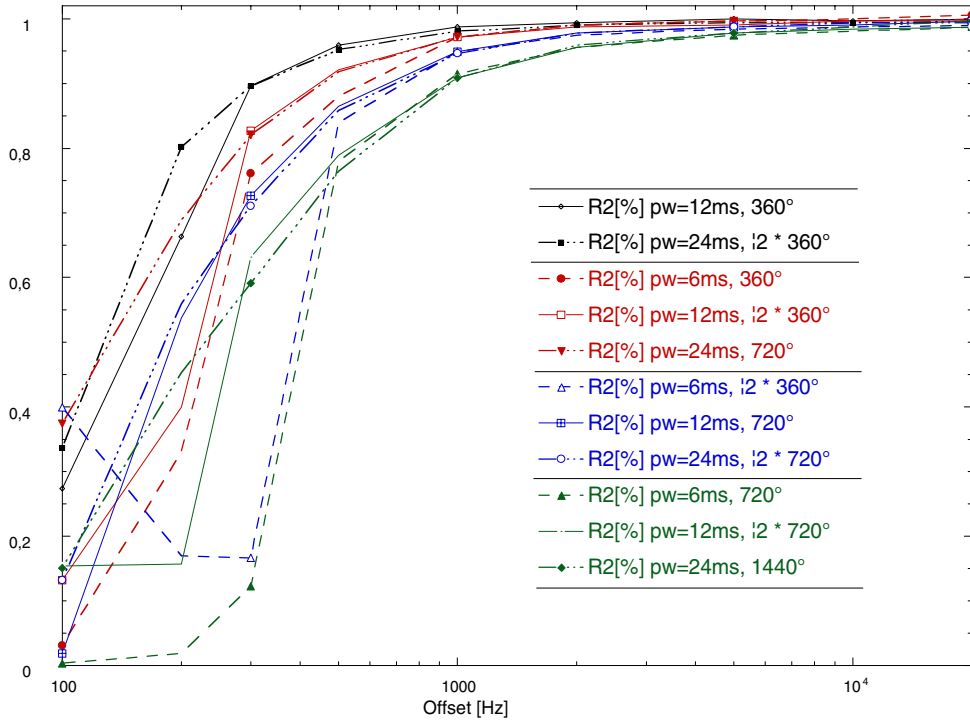


Figure 7.1 The MT-effect and direct saturation for the same RF-power but different pulse lengths and flipangles. The signal is normalised to the reference measurement with zero degree flipangle. Comparing the MT effect for one pulse chain and an other, where the pulse width and the flipangle is increased with a factor of 2 and $\sqrt{2}$ respectively, the MT saturation should be the same. This is shown for offset frequencies larger than approximately 700Hz, for lower offsets direct saturation of the H_f -pool is present.

For offsets greater than 0.5 kHz the decrease of the H_f -signal by saturation of H_f proved to be roughly dependent on the power integral of the saturation pulses

$$\int B_i^2(t)dt \propto A^2 T \propto \frac{\text{flipangle}^2}{T} \quad \text{eq. 7.1}$$

, where A is the rf amplitude and T the pulselength. This means that the same MT effect can be achieved at lower flipangle if short pulses are used. This dependence $MTR \propto A^2$ has been shown for rectangular pulses (12) but seems to be true even for the shaped pulses we used. Comparing the MT effect for one pulse chain with an other, where the pulse width and the

flipangle is increased with a factor of 2 and $\sqrt{2}$ respectively, the MT saturation is the same. This behaviour may be used to distinguish MT saturation from direct saturation.

At 0.5kHz one may see a small difference in saturation between pulses with similar power but different pulse widths. This is probably already the effect of direct saturation by the shorter pulses because of their larger bandwidth ($bw \sim 1/pw$). At smaller frequency offsets the effect of direct saturation can clearly be seen.

Because the MT effect is quite small for larger offset frequencies, we should saturate as close as possible in frequency offset without affecting the H_f pool directly. This, however, we have to avoid direct saturation even at the cost of smaller MT effect, because our model does not include direct saturation of the H_f -pool. In principle, shorter pulses would yield a better saturation and a possibility of faster pulse repetition, which in turn also improves the MT effect, see figure 7.2. However system restrictions are also imposed on the maximum allowable amplitude so we were forced to compromise and the pulse of 12ms pulsewidth and offset of 1000Hz was chosen for off resonance saturation.

The plot in figure 7.2 shows the signal for a different number of pulses but constant saturation time at different offset frequencies. It is evident that the MT effect is bigger for fast pulse repetitions, i.e. small TD. For offsets greater than 5kHz, an almost linear dependence is seen indicating that we are far away from reaching a constant value. At 1kHz a roughly exponential behaviour is seen and it may, compared to the other offsets(5,10 and 20kHz), relatively fast converge to its minimum value. The fact that no one before has studied the strong dependence of the MT effect on the pulse repetition TD, motivated us to concentrate on this parameter.

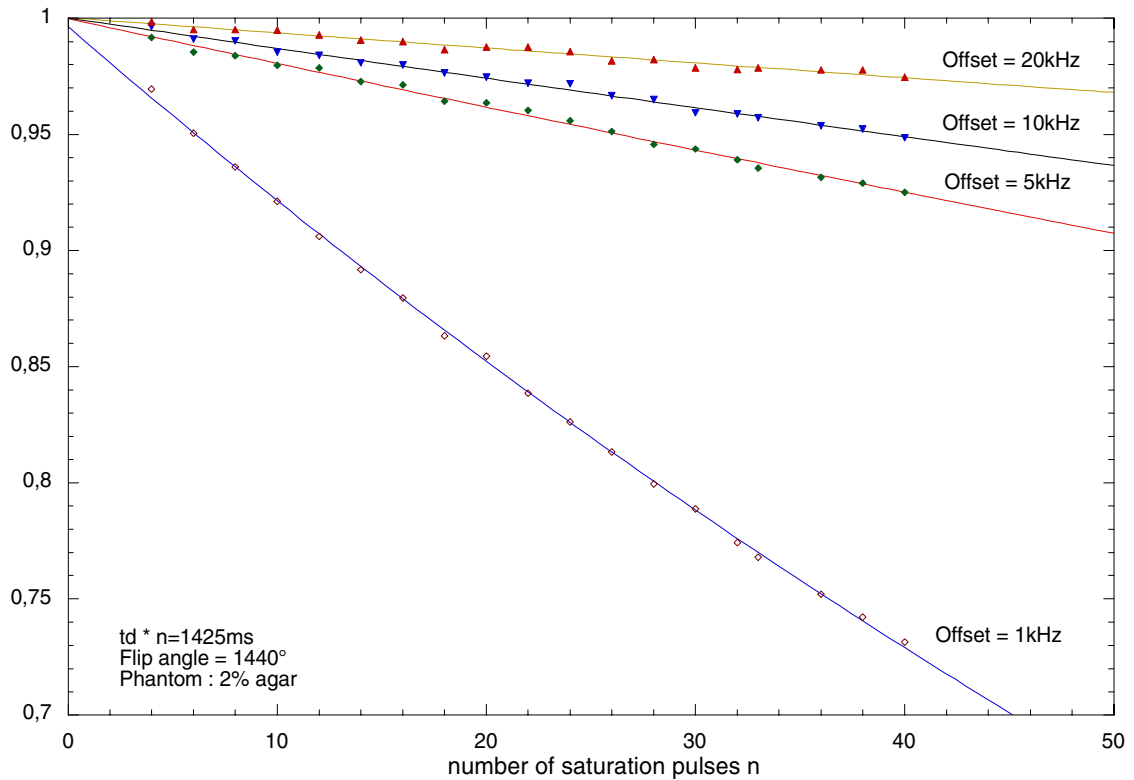


Figure 7.2 The MT saturation for different frequency offsets in a 2% agar phantom. The total length of the saturation pulse chain was hold constant at 1425ms. This means that $n=4$ and $n=40$ corresponds to $TD=320$ and $TD=35$ ms respectively. Hypothetically the minimum value is reached after 500,3000,4000 and 7000 pulses respectively.

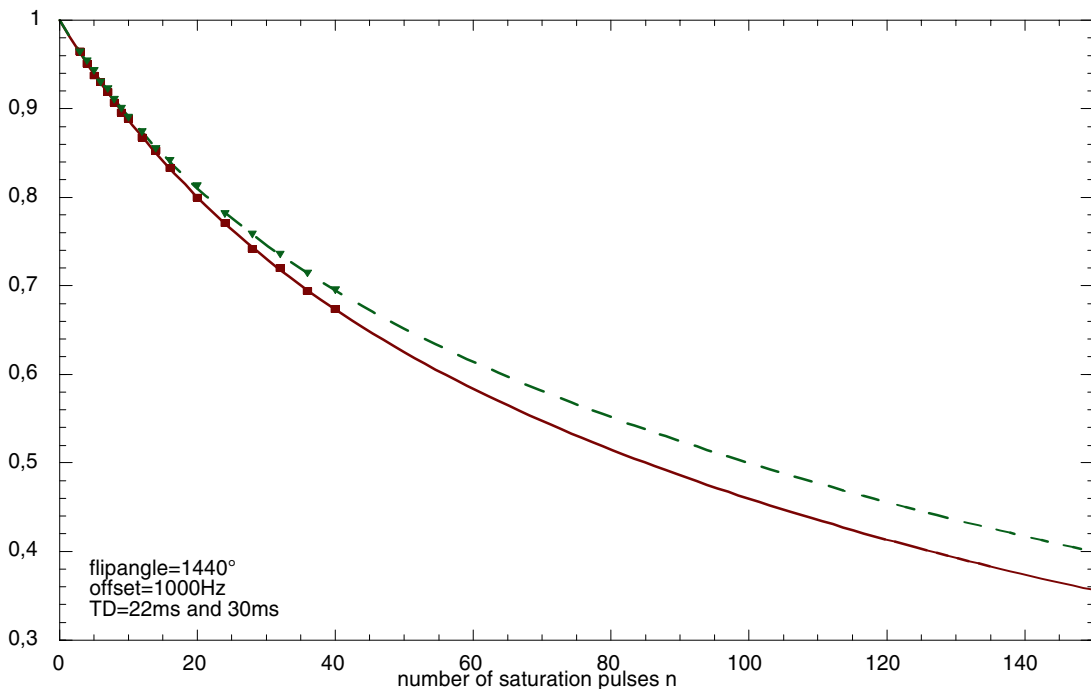


Figure 7.3 A 2% agar phantom shows a biexponential approach to steady state of 0.12 and 0.14 value of the normalised signal. However the amplitudes of μ_1 and μ_2 are very different from those obtained in vivo and they did not match the equations in chapter 3.5.

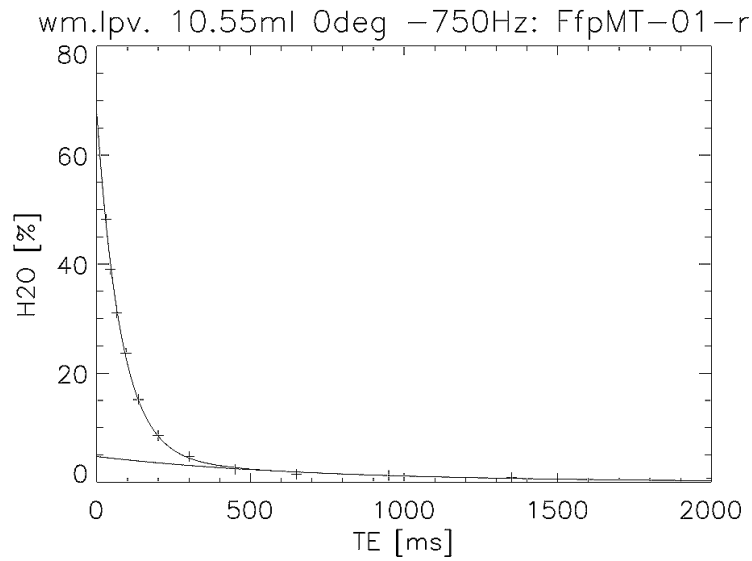
A measurement in agar seen in figure 7.3 shows that we are far away from achieving steady state, which is favourable because of its well defined stable condition. The steady state condition seems equally far away to be achieved for both TD values. Agar shows a biexponential approach to steady state of 0.12 and 0.14 value of the normalised signal. However the amplitudes of μ_1 and μ_2 are very different from those obtained in vivo and they do not match the equations in chapter 3.5. From this we concluded that, despite its common use, that agar is not a suitable phantom to mimic in vivo conditions.

In vivo measurements

The first problem was to find out whether the CSF is really not affected by the MT saturation. In vivo measurements it is generally believed that the CSF does not show any MT effect. Therefore we have to correct our MT measurements for the CSF content of the VOI, especially in grey matter, where the CSF contribution is large. The volume of the CSF compartment are determined by T_2 -relaxation measurements and absolute quantification of the signal, required T_2 -values are approximately 10, see fig. 7.4.

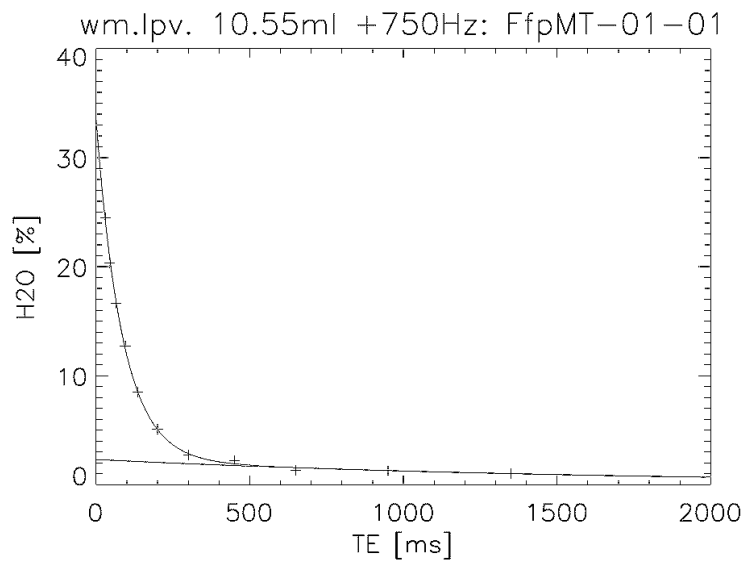
In fig. 7.4 two T_2 relaxation curves from a VOI in periventricular white matter are displayed, one showing the biexponential fit for the reference signal(0°) and the other after saturation($n=20$, $TD=75ms$, not in scale). The MT saturation effect and the separation of the compartments are shown by these measurements.

The difference in CSF content between the reference and saturated signal (5% and 2%, fig. 7.4) is coupled to the fitted relaxation times(700ms and 1640ms). We are measuring not enough data points at larger TE values, giving the fit too much freedom to induce variations in the CSF relaxation time. However, by calculating the CSF signal at a larger TE, we can get a more correct measure of the CSF signal.



h2o fit: $CSF \cdot \exp(-t/T2_csf) + TW \cdot \exp(-t/T2_tw)$

TG=	CSF=	4.70450 %	2.70156
93.0000	TissueSignal=	63.0202 %	2.48796
TG_lok=	missing=	32.2753 %	
88.6000	T2(csf)=	699.979 ms	478.105
ext.scl.R2=	T2(tw)=	78.3376 ms	7.17106
1.04050	TissueVolume=	10.0537 ml of	10.5500 ml
Accum=	true TissueSignal=	66.1314 % of	Tissue
32.0000	true missing=	33.8686 % of	Tissue



h2o fit: $CSF \cdot \exp(-t/T2_csf) + TW \cdot \exp(-t/T2_tw)$

TG=	CSF=	2.31121 %	1.47794
93.0000	TissueSignal=	31.1979 %	1.91528
TG_lok=	missing=	66.4909 %	
88.6000	T2(csf)=	1641.53 ms	2053.65
ext.scl.R2=	T2(tw)=	85.4648 ms	12.0593
1.04050	TissueVolume=	10.3062 ml of	10.5500 ml
Accum=	true TissueSignal=	31.9360 % of	Tissue
32.0000	true missing=	68.0640 % of	Tissue

Figure 7.4 T_2 measurements in periventricular white matter for a) reference signal (0°) and b) the saturated signal. T_2 times of CSF are 700ms and 1640ms and correlate to the amplitude of the fitted signal.

Figure 7.5 shows the extrapolated CSF signal at 0ms TE and the CSF signal at 450ms of 15 consecutive measurements, with different offset frequencies, where the CSF signal at long TE appears to be unaffected by the MT saturation. The variations are thereby reduced from absolute 3% to 1%. However, the relaxation method did not deliver the relaxation time with acceptable accuracy. And therefore the T_2 times shall not be considered. Because of these circumstances we avoided CSF contributions of the measured VOI. In white matter this is relatively easy, while it for grey matter is unavoidable. Therefore the grey matter MT studies may not properly correspond to the expected MT behaviour and they must also, for their CSF partial volume, be corrected.

Simulations have shown that the CSF corrected water signal (true tissue water) is nearly independent over a wide range of CSF relaxation times. Therefore it is still possible to use the tissue water amplitude determined by the relaxation method. The change in the left four points for the offset dependence of the saturation shown in fig.7.5 is probably due to patient movement at the end of the 2-hour examination.

Brain tissue water shows the characteristic effect of irradiation frequency and it should be noted that the saturation of the brain tissue is much stronger than in the 2% agar phantom (cf. fig. 7.1). The saturation shows symmetrical dependence in offset frequency within the experimental error (5%). Our measurements on 40kHz offset did not show any measurable direct saturation of H_f , which state the fact that the sample theorem is fulfilled, i.e. 12 μ s sampling of pulses is sufficient.

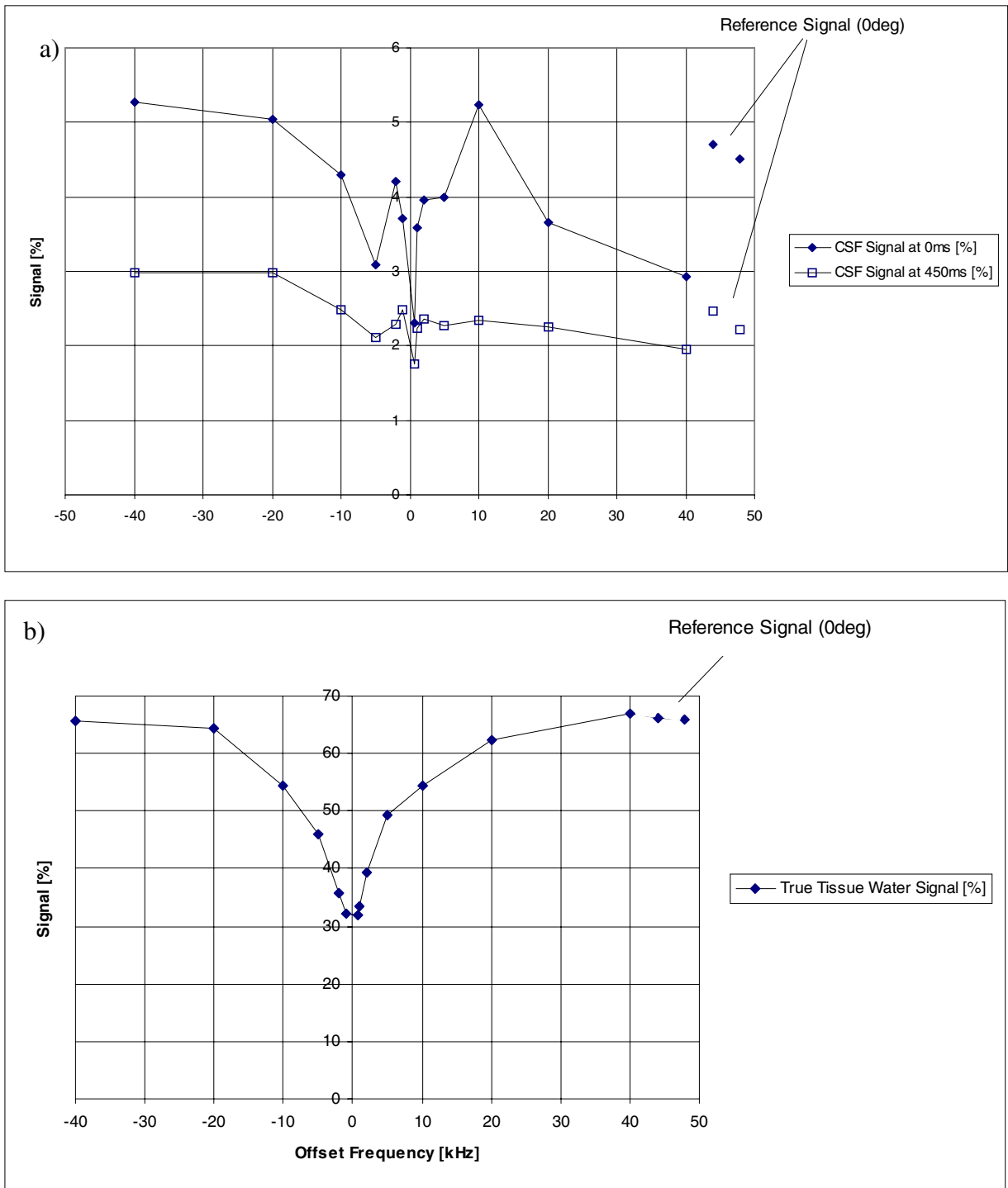


Figure 7.5 Ffp-01 white matter (the same as in figure 7.4) a) The CSF content seemed to be unaffected by the MT saturation while b) the brain tissue water shows the characteristic effect of irradiation frequency. Note that the saturation of the brain tissue is symmetrical in frequency. The reference signal for 0° flip angle corresponds to the signal without MT saturation and corresponds as well to the CSF signal with MT(a) as the tissue water signal with MT(b). The irregular shape of the CSF measurements for offset frequencies below 0Hz is probably due to patient movements.

In human brain matter we came very close to steady state in contrast to the agar phantom measurements previously described. Therefore a reliable extrapolation towards the steady state was possible giving the value of MTR_{ss} (correlation coefficient $r > 0.997$), which is shown in fig. 7.6.

However, the closeness to steady state varied with the pulse repetition time. Steady state was almost reached for TD of 50ms. Otherwise the steady state is not reached for two kind of reasons: the first is the limited preparation time, which is the restriction for slow repetition, the other reason is the limited number of applied saturation pulses, which is the restriction for fast repetition (see chapter 6.2). As seen in figure 7.6, for small TD values it takes more pulses to reach steady state. But if the time of this process is considered, steady state is reached earlier in time for fast repetition. The smaller TD the more saturation is created of the H_f , which is in accordance with fig. 7.2. It should therefore be noted that MTR_{ss} is strongly dependent on TD revealing the fact that greater saturation can be obtained by faster pulsing until SAR becomes to high.

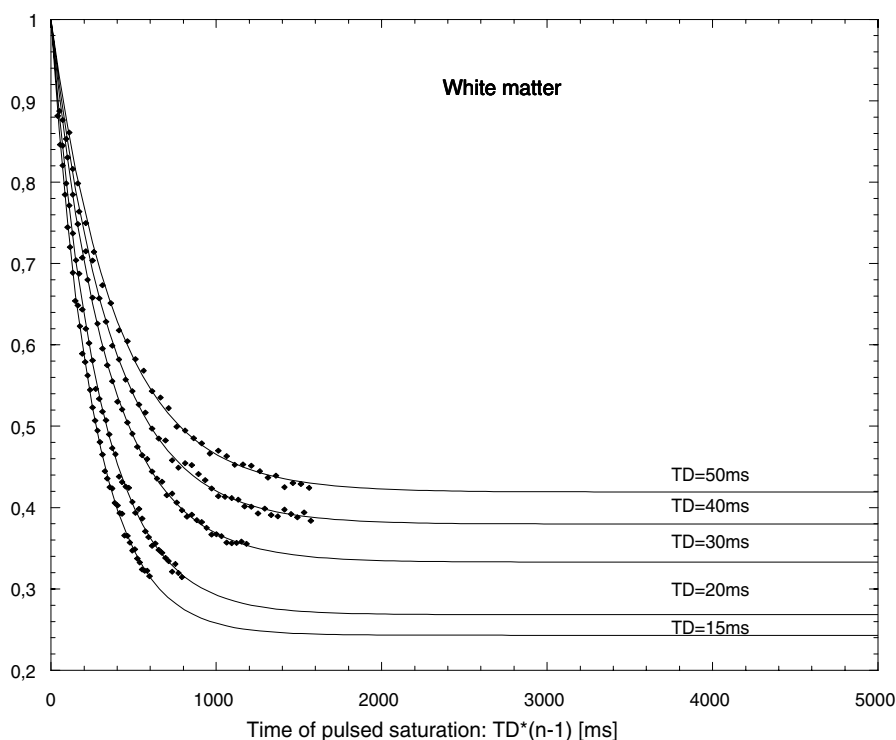


Figure 7.6 The approach to steady state for different TD values in white matter. The plots in figure 7.6-7.8 show the best experiments for white and grey matter studies. For TD=50 the maximum number of pulses n is 32, because of maximum saturation time of 1625ms, while the n is 40 for TD<40ms. The plot shows that high TD values achieve steady state faster depending on number of pulses. But if the total length of the saturation time is considered, fast repetition is faster, but with the distinction that more pulses is emitted. The conclusion is that higher pulse rate is ineffective considering reaching steady state. However, the lower TD the stronger saturation is received.

For TD values in the range between 15ms and 100ms steady state is approximately reached after 130-60 pulses respectively, which is a lot compared to the number of phase encoding steps in a standard MRI experiment. For this reason MT contrast detected in MRI may involve considerable contributions from the approach to steady state.

Lowering the flip angle would make the steady state condition easier to accomplish, sacrificing the MTR. If the pulse width makes shorter we can pulse faster sacrificing the power of the pulse and thus the saturation level.

The grey matter VOI's contained a considerable amount of CSF in brain tissue of the sulci and the extracellular space (which is only 3% in white matter), which the calculations were corrected for. Moreover there are more vessels in grey than in white matter. White matter can be assumed to better correspond to the two-pool model because of its better homogeneity. For this reason we concentrated on white matter, consequently we have more statistics for white matter.

A biexponential approach to steady state, as predicted by theory (cf. eq.3.19), can be fitted for the *in vivo* measurements. However, μ_2 is relatively small compared to μ_1 (0.3 and 0.9) and can only be detected in the first four points. Therefore it can not be determined accurately. The approach to steady state seems to be monoexponential, see fig.7.6. Excluding the μ_2 from the fit neither changed the steady state nor the dominant μ_1 within the accuracy of the measurement. However, the lack of μ_2 will prevent us to determine the constants of the kinetic model, see chapt 3.6.

In white matter the MTR_{ss} shows very good accuracy of the theoretical expectations, whereas the grey matter measurements proved to be more difficult to fit, which can be due to its more complex tissue composition.

On the fact that the major part of our measurements in grey tissue matter showed a deviating approach to steady state, the accuracy of the fits of μ_1 and MTR_{ss} dependence of TD will at larger extent be affected than for the white matter measurements. Signal oscillations seemed sometimes follow a certain multiple of saturation pulses n , which can be a result of stimulated echoes. Some of the data was so bad that we could not use them. Due to relatively few experiments in grey matter could not decide whether these variations are due to system instability, eddy currents, stimulated echoes or patient movement.

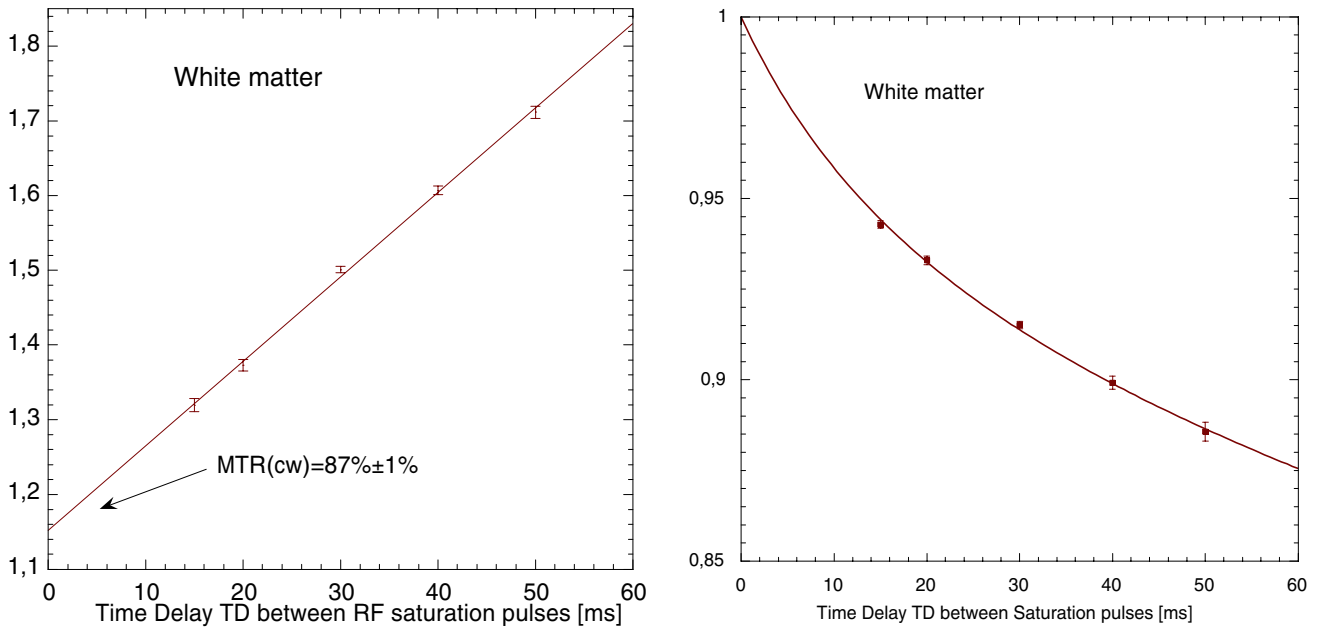


Figure 7.7 Curvefits corresponding the MTR_{ss} ($r=0.998$) and the μ_1 ($r=0.999$) dependence for estimation of the MTR_{cw} and the kinetic constants k_r, T_{1f} and k_r, T_{1ar}, μ_2 could not be fitted accurately.

Although steady state not was reached and μ_2 could not be fitted and accurate determined, the quantitative measurements of pulsed MT *in vivo* in white and grey matter respectively corresponded well to the theory described in chapter 3.6. The measurements only used TD values ranging between 15ms and 100ms according to the approximation $TD \ll k_r, T_{1f}, T_{1ar}$. The dependence of the steady state value MTR_{ss} and the μ_1 on pulse repetition are excellently observed. The correlation coefficient for the experimental data was as much as $r > 0.995$ for all measurements, see table 7.1. The linearity of the MTR_{ss} was very good even for larger TD values, whereas the μ_1 seemed harder to fit. Therefore μ_1 should be measured at smaller TD.

Measurements concerning saturation pulses with different flipangles show that for small differences in flipangles a relatively high difference of MTR_{ss} is achieved, e.g. 10% absolute difference between 1080° and 1440° . To achieve an as effective suppression of tissue as possible it is therefore crucial to use the maximum allowable power with the saturation pulses.

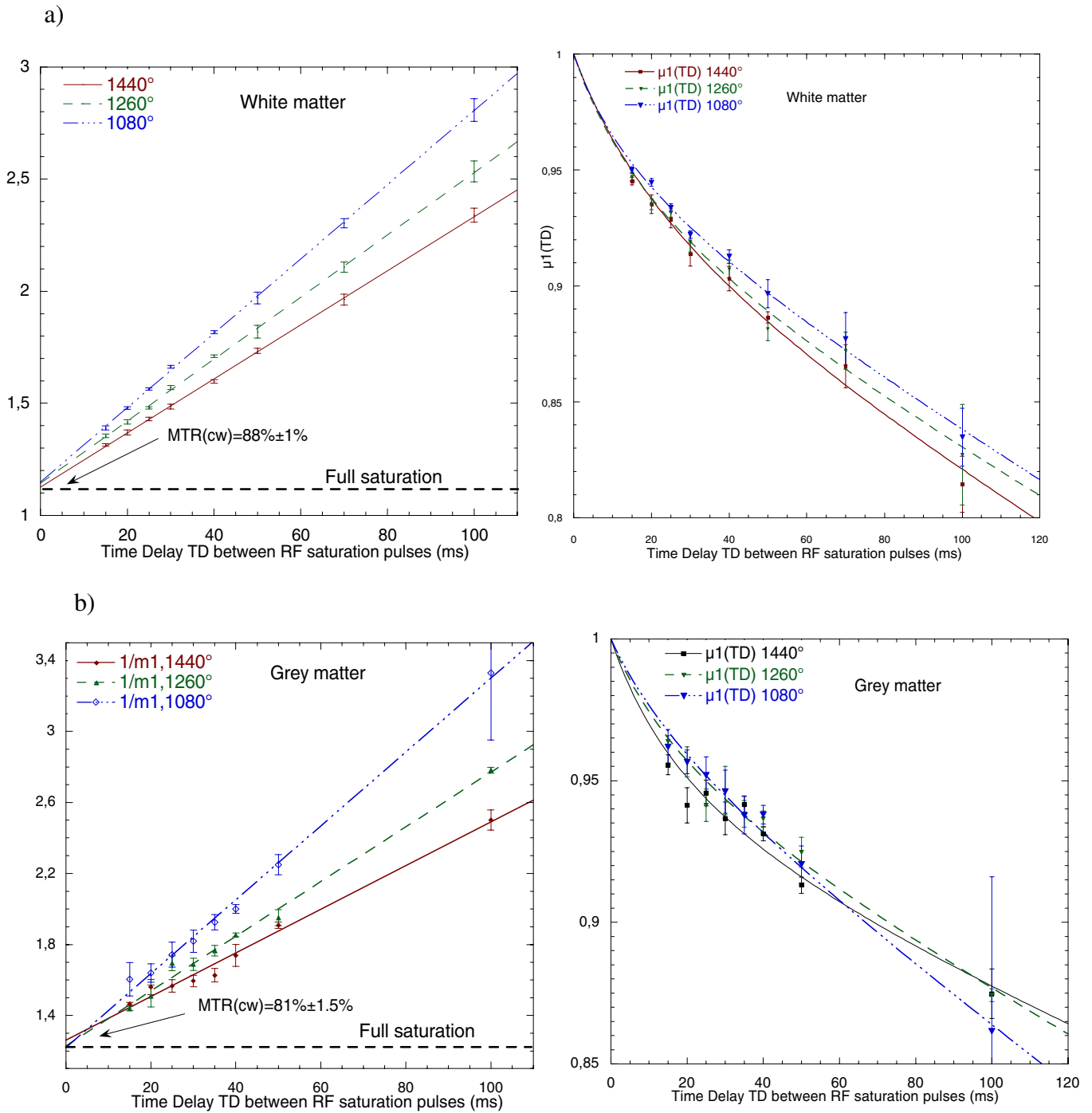


Figure 7.8 Curvefits of the MTR_{ss} and μ_1 values for different flipangles, i.e. saturation pulses with different integrated power, in white and grey matter. As predicted by theory MTR_{cw} is independent of the arbitrary saturation α . a) White matter measurements, the plots corresponds to Ffp-10 b) Grey matter measurements, the content of CSF is corrected for (Ffp-09).

Using the MTR_{ss} measurements it is possible to calculate the expected cw saturation. This is achieved by an extrapolation of MTR_{ss} 's linear dependence over TD, mentioned in chapt. 3.6. Figure 7.8a) and b), shows the same MTR_{cw} value, i.e. same intersection of the y-axis, for

different flipangles of the saturation pulses. As predicted in the theory, MTR_{cw} is independent of the arbitrary saturation α and can therefore be used to compare MT effects quantitatively even for different saturation paradigms. Because MTR_{ss} and μ_1 is coupled to each other it is not surprising that grey matter shows less accuracy of the theoretical model.

Values of the MTR_{cw} obtained from the linear approximation of MTR_{ss} over TD for white matter were $87.7 \pm 2.3\%$ (mean \pm SD n=12, range 85-93%) and $82.5 \pm 2.0\%$ (n=6, range 79-84%) for grey matter after correction for CSF partial volume, see table 7.1-7.4. This value of MTR is much higher than earlier published values obtained in MRI, which range between 36-48% and 28-39% for white and grey matter respectively for different techniques (5). However, evaluations of the MTR in MRI studies are less dependent on the CSF contribution than our studies, which is due to no or less partial volume effect of CSF, because of smaller voxel size.

Table 7.1 Extrapolated values of MTR_{cw} from the linear fit of $MTR(TD)$ measurements in white matter. Calculated mean and standard deviations of MTR_{cw} is calculated for all flipangles and measurements in white matter. R= correlation coefficient.

White	Ffp-03		Ffp-04		Ffp-05		Ffp-06		Ffp-08		Ffp-10		Ffp-14	
	MTR_{cw}	R	MTR_{cw}	R	MTR_{cw}	R	MTR_{cw}	R	MTR_{cw}	R	MTR_{cw}	R	MTR_{cw}	R
1490°					0.85	0.955								
1440°	0.93	0.999	0.89	0.999	0.86	0.992	0.84	0.885	0.85	0.991	0.89	0.999	0.88	0.998
1390°					0.85	0.994								
1260°							0.86	0.924	0.89	0.999	0.88	0.999		
1080°							0.77	0.836	0.90	0.997	0.87	0.999		
	Mean MTR_{cw}				Std									
All flipangles	0.88				0.023									

Table 7.3 Extrapolated values of MTR_{cw} from the linear curve fit of $MTR(TD)$ measurements in parietal grey matter(corrected for CSF partial volume). Calculated mean and standard deviations of MTR_{cw} is calculated for all flipangles and measurements in grey matter.

Grey matter	Ffp-09		Ffp-11	
	MTR_{cw}	R	MTR_{cw}	R
1440°	0.83	0.996	0.83	0.994
1260°	0.84	0.996	0.79	0.998
1080°	0.84	0.999	0.82	0.996
Mean values	Mean MTR_{cw}		Std	
All flipangles	0.825		0.019	

From the fitted parameters MTR_{ss} and μ_1 we are able to calculate the values of the kinetic constants. However, as mentioned above the time constant μ_2 were not able to accurately be

determined and as a result we lose some information of the process. This will in fact prevent us to determine the constants of the kinetic model, especially T_{ar} and α .

The kinetic constants in the "free" pool was determined to $T_{1af}=209\pm 17\text{ms}$, $T_{1f}=1620\pm 170\text{ms}$ and $k_f=4.2\pm 0.4\text{s}^{-1}$ (n=9) in white matter, and for grey matter to $T_{1af}=248\pm 17\text{ms}$, $T_{1f}=1430\pm 200\text{ms}$ and $k_f=3.3\pm 0.2\text{s}^{-1}$ (n=6). Further investigations have to be done for grey matter especially. For the restricted mobile pool of magnetisation $k_r \cdot T_{1ar}$ were calculated to 0.85 ± 0.04 and 0.98 ± 0.05 for white and grey matter respectively, see table 7.5-7.8.

In MRI the $T_1(\text{g.m.}) > T_1(\text{w.m.})$ but here the $T_{1f}(\text{g.m.}) < T_{1f}(\text{w.m.})$. This can be due to errors in the corrections of the CSF content but also an effect of partial saturation of the H_r -pool in MRI can be one reason.

MT measurements has very good reproducibility for a given technique, which several articles show, but they all show great differences in MTR. This report makes it possible to compare cw and pulsed techniques with each other to get a better understanding of the differences in MTR values.

Table 7.4 Rate constants for white matter and calculated mean and standard deviations for rate constants for white matter.

White matter								
Ffp-04	k_f [s^{-1}]		T_{af} [ms]		T_{1f} [ms]		$T_{ar} \cdot k_r$	
1440°	0.00402		221		1947		0.790	
Ffp-05	0.00397		215		1473		0.850	
1440°	0.00367		235		1706		0.797	
1390°	0.00388		219		1460		0.862	
Ffp-10	0.00450		197		1750		0.863	
1260°	0.00441		198		1582		0.875	
1080°	0.00426		204		1561		0.877	
Ffp-14	0.00489		179		1484		0.890	
Mean values	k_f [s^{-1}]	Std	T_{1af} [ms]	Std	T_{1f} [ms]	Std	$T_{ar} \cdot k_r$	Std
1490° (n=1)	4.0		215		1473		0.85	
1440° (n=5)	4.3	0.5	208	25	1722	190	0.84	0.05
1390° (n=1)	3.9		219		1460		0.86	
1260° (n=1)	4.4		198		1582		0.88	
1080° (n=1)	4.3		204		1561		0.88	
All flipangles	4.2	0.4	209	17	1620	170	0.85	0.04

Table 7.6 Rate constants for grey matter in Ffp-09 and Ffp-11 (corrected for CSF partial volume) and calculated mean and standard deviations for rate constants for grey matter for all flipangles

Grey matter								
Ffp-09	k_f [s^{-1}]		T_{1af} [ms]		T_{1f} [ms]		$T_{ar} * k_r$	
1440°	3.7		226		1366		1.02	
1260°	3.4		245		1509		0.99	
1080°	3.2		261		1621		0.96	
Ffp-11								
1440°	3.1		266		1606		0.91	
1260°	3.4		229		1088		1.05	
1080°	3.1		262		1415		0.96	
Mean values	k_f [s^{-1}]	Std	T_{1af} [ms]	Std	T_{1f} [ms]	Std	$T_{ar} * k_r$	Std
All flipangles	3.3	0.2	248	17	1434	200	0.98	0.05

Concerning the system restrictions mentioned in chapt. 6.2, improvement of hardware and some modifications of the saturation sequence should improve and optimise the system for our purposes, and hopefully no need for exponential extrapolation of the measured MTR values. This will in turn give better and more reliable data of the pulsed MT time dependence, its rate constants and relaxation time determinations.

8. Conclusion

Assuming a 2-pool model for magnetisation transfer using a conventional scanner and a pulsed saturation technique with short repetition we demonstrated that it is possible to derive the maximum MT saturation (MTR_{cw}) and to determine the kinetic constants for free water. So far this has been possible by using cw irradiation on experimental MR systems. The MT effect was strongly dependent on the pulse repetition (TR) and the highest MTR were obtained for short TR. Thus, limitation of transmitter power on clinical system can be overcome using short repetition.

By extrapolation of MTR_{ss} we can determine the expected maximum saturation MTR_{cw} and it is shown that MTR_{cw} is independent of the arbitrary saturation α and can therefore be used to compare MT effects quantitatively even for different saturation paradigms and MR scanners.

There were individual differences in MT parameters between different Ffp's in white and grey matter. For white matter the 2-pool model showed to be accurate but for the grey matter it seemed to be bad. This is possible due to a more complicated compartmentation in grey matter and the fact that the relaxation method not is accurate enough to separate the MT effect of the different compartments.

If the most severe system restrictions, which limits the applied number of pulses and the total saturation time, could be overcome, a fully achieved steady state would be obtained. This would yield a better accuracy of the MT measurements. By lowering the flipangle the α value, i.e. fraction of magnetisation M_r left after one saturation pulse, will be less, yielding a bigger μ_2 (and μ_1). Thus, a determination of all the MT parameters would be provided, where the saturation fraction α especially would be of interest, in order to optimise the efficiency of the saturation pulses. Therefore, with further investigations of the experiments a complete determination of the MT process *in vivo* might be possible. The result of an understood MT saturation technique could be a quantitative MT Imaging method, in which the spatial distribution of the MT process is shown.

9. APPENDIX A : EPIC Code of the MT Preparation Sequence

@cv MTSuppressCV

```

/***** Solvent MTSuppression Acquisition CVs *****/
int mtsup_atten = 1 with {1,100,1,VIS, "multiplier for extra attenuator",};
short mtsuppress = 0 with {0,1,0,VIS,"1=ON, 0=OFF for suppression",};
short mtsup = 0 with {0,1,1,VIS,"1=ON, 0=OFF for suppression",};
short mtsup_grads;
short mtsup_rf;
short mt = 0 with {0,1,0,VIS,"1=ON, 0=OFF for MT-suppression",};
short sincsup = 1 with {0,1,1,VIS,"1=sinc, 0=slr MTsup pulses",};
int pulse_rfmt;
float nom_bw_rfmsup;
float nom_fl_rfmsup;
float bw_rfmsup = 50.0 with {10,1000,50,VIS,"bandwidth of MT-sup pulses",};
float offset_rfmsup = 1000.0 with {-100000,100000,1000,VIS,"offset of MT-sup pulses",};
float bw_rfmt = 50.0 with {10,1000,50,VIS,"bandwidth of rfmt",};
float flip_rfmt = 14400.0 with {0,15000,14400,VIS,"desired flip angle for rfmt",};
int res_rfmsup = 1000;

float m_gxcmt01 = 1.0 with {-1,1,1,VIS,"gc01 x multiplier",};
float m_gycmt01 = 1.0 with {-1,1,1,VIS,"gc01 y multiplier",};
float m_gzgmt01 = 0.0 with {-1,1,0,VIS,"gc01 z multiplier",};
float m_gxcmt02 = 0.0 with {-1,1,0,VIS,"gc02 x multiplier",};
float m_gycmt02 = 1.0 with {-1,1,1,VIS,"gc02 y multiplier",};
float m_gzgmt02 = 1.0 with {-1,1,1,VIS,"gc02 z multiplier",};
float m_gxcmt03 = 1.0 with {-1,1,1,VIS,"gc03 x multiplier",};
float m_gycmt03 = 0.0 with {-1,1,0,VIS,"gc03 y multiplier",};
float m_gzgmt03 = 1.0 with {-1,1,1,VIS,"gc03 z multiplier",};

int pw_dattenmton = 3; /* atten logic ssp packets */
int pw_dattenmtoff = 3;

/***** Pulse Control CVs *****/
/* MTSuppress CV's*/
int t_mtshimrf = 500us with {100us,19ms,500us,VIS,"shim time around rf pulses for MTprep-pulses",};
int t_mtsp = 1ms with {1,20ms,1ms,VIS, "MTsuppression rf/spoiler spacing",};
int wft_mtst01,wft_mtst02;
int t_mtst01,t_mtst02;
int tstr_mtst01,tstr_mtst02;
int wft_mt;
int t_mt;
int tstr_mt;
int wft_td;
int td;
int tstr_td;
int n_rf=3;
int wft_mtend;
int t_mtend;
int tstr_mtend;
int t_mtsup;
int temp;
int pw_gcmt01,pw_gcmt02,pw_gcmt03;
float a_gcmt01,a_gcmt02,a_gcmt03;
/* Suppress CV's*/
int t_shimrf = 500us with {100us,19ms,500us,VIS,"shim time around rf pulses",};
int t_c0sp = 1ms with {1,20ms,1ms,VIS, "suppression rf/spoiler spacing",};
int wft_st01,wft_st02;
int t_st01,t_st02;
int tstr_st01,tstr_st02;
int wft_0102;
int t_0102;
int tstr_0102;
int wft_0203;

```

```

int t_0203;
int tstr_0203;
int wft_03end;
int t_03end;
int tstr_03end;
int t_sup;
int pw_gc01,pw_gc02,pw_gc03;
float a_gc01,a_gc02,a_gc03;

@host MTSuppressEval

/*****
Pulses and crushers for solvent MTsuppression
*****/

/* here set the flags for suppression*/

if ((specnuc == 1) && (scanmode == 1))
    mtsuppress = 1;
else
    mtsuppress = 0;

if (specnuc == 1)
    mtsup = 1;
else
    mtsup = 0;

if ((scanmode == 1) && (mtsup == 1))
    mtsup_grads = 1;
else
    mtsup_grads = 0;

if ((scanmode == 1) && (mtsup == 1) && (mtsuppress==1))
    mtsup_rf = 1;
else
    mtsup_rf = 0;

if (mt == 1){
    mtsuppress = 1;
    mtsup = 1;
    mtsup_grads = 1;
    mtsup_rf = 1;
}
else{
    mtsuppress = 0;
    mtsup = 0;
    mtsup_grads = 0;
    mtsup_rf = 0;
}

if (sincsup == 1) /*sinc-pulse*/
{
    nom_bw_rfmsup = 1620.0;
    if (tgdoube == 1)
        nom_fl_rfmsup = 128.4 * 2;    /*before 42.76*/
    else
        nom_fl_rfmsup = 128.4;

    /* factors for sinc */
    rfpulse[RF_MTSUP_SLOT].area = 0.1000;
    rfpulse[RF_MTSUP_SLOT].abswidth = 0.2948;
    rfpulse[RF_MTSUP_SLOT].effwidth = 0.4324; /*0.1806*/
    rfpulse[RF_MTSUP_SLOT].dtycyc = 0.9960; /*0.4400*/
    rfpulse[RF_MTSUP_SLOT].maxpw = 0.9960; /*0.4080*/
}
else /*slr-pulse*/
{

```

```

nom_bw_rfmsup = 1340.0;
if (tgdoube == 1)
    nom_fl_rfmsup = 128.4 * 2;
else
    nom_fl_rfmsup = 128.4;          /* factors for slr */
rfpulse[RF_MTSUP_SLOT].area = 0.6112; /*0.5707*/
rfpulse[RF_MTSUP_SLOT].abswidth = 0.5707;
rfpulse[RF_MTSUP_SLOT].effwidth = 0.4324;
rfpulse[RF_MTSUP_SLOT].dtycyc = 0.9960;
rfpulse[RF_MTSUP_SLOT].maxpw = 0.9960;
}

/*****
Bookkeeping for pulses and grads
*****/

if (mtsup_rf == 1)
{
    rfpulse[RF_MTSUP_SLOT].num = n_rf;
}
else
{
    rfpulse[RF_MTSUP_SLOT].num = 0;
}

if (mtsup_grads == 1)
{
    gradx[GXCMT01_SLOT].num = 1 * m_gxcmt01;
    grady[GYCMT01_SLOT].num = 1 * m_gycmt01;
    gradz[GZCMT01_SLOT].num = 1 * m_gzcm01;

    gradx[GXCMT02_SLOT].num = 1 * m_gxcmt02;
    grady[GYCMT02_SLOT].num = 1 * m_gycmt02;
    gradz[GZCMT02_SLOT].num = 1 * m_gzcm02;

    gradx[GXCMT03_SLOT].num = 1 * m_gxcmt03;
    grady[GYCMT03_SLOT].num = 1 * m_gycmt03;
    gradz[GZCMT03_SLOT].num = 1 * m_gzcm03;
}
else
{
    gradx[GXCMT01_SLOT].num = 0;
    grady[GYCMT01_SLOT].num = 0;
    gradz[GZCMT01_SLOT].num = 0;

    gradx[GXCMT02_SLOT].num = 0;
    grady[GYCMT02_SLOT].num = 0;
    gradz[GZCMT02_SLOT].num = 0;

    gradx[GXCMT03_SLOT].num = 0;
    grady[GYCMT03_SLOT].num = 0;
    gradz[GZCMT03_SLOT].num = 0;
}

/* pulse widths and amplitudes for MTsuppression rf pulses and shims */

bw_rfmsup = 75.0;

bw_rfimt = bw_rfmsup;
pw_rfimt = 12*1ms;          /*970714*/
/*pw_rfimt = (int)(nom_bw_rfmsup/bw_rfimt)*1ms;*/ /*int to round off to ms*/

pw_gxmtshim01 = 2*t_mtshimrf + pw_rfimt;
pw_gymtshim01 = 2*t_mtshimrf + pw_rfimt;
pw_gzmtshim01 = 2*t_mtshimrf + pw_rfimt;

```

```

pw_gxmtshim02 = 2*t_mtshimrf + pw_rfnt;
pw_gymtshim02 = 2*t_mtshimrf + pw_rfnt;
pw_gzmtshim02 = 2*t_mtshimrf + pw_rfnt;

pw_gxmtshim03 = 2*t_mtshimrf + pw_rfnt;
pw_gymtshim03 = 2*t_mtshimrf + pw_rfnt;
pw_gzmtshim03 = 2*t_mtshimrf + pw_rfnt;

a_gxmtshim01 = (float)(mrsavs_gxmtshim*cfpcmfs)/(float)(max_pg_iamp);
a_gymtshim01 = (float)(mrsavs_gymtshim*cfpcmfs)/(float)(max_pg_iamp);
a_gzmtshim01 = (float)(mrsavs_gzmtshim*cfpcmfs)/(float)(max_pg_iamp);

a_gxmtshim02 = (float)(mrsavs_gxmtshim*cfpcmfs)/(float)(max_pg_iamp);
a_gymtshim02 = (float)(mrsavs_gymtshim*cfpcmfs)/(float)(max_pg_iamp);
a_gzmtshim02 = (float)(mrsavs_gzmtshim*cfpcmfs)/(float)(max_pg_iamp);

a_gxmtshim03 = (float)(mrsavs_gxmtshim*cfpcmfs)/(float)(max_pg_iamp);
a_gymtshim03 = (float)(mrsavs_gymtshim*cfpcmfs)/(float)(max_pg_iamp);
a_gzmtshim03 = (float)(mrsavs_gzmtshim*cfpcmfs)/(float)(max_pg_iamp);

/*flip_rfnt = mrsaws_flip03;*/ /* mrsaws_flip03 set by AWS */

/* pointers for rf pulses */
if (sincsup == 0) /*slr-pulse*/
{
    pulse_rfnt = -1;
}
else
{
    pulse_rfnt = 0; /*IMin(2,7,(IMax(2,0,(int)((flip_rfnt-630)/100))))*/
}

if (mtsup_rf == 1)
{
    a_rfnt = flip_rfnt/(10*nom_fl_rfntsup)*1.0ms/pw_rfnt;

    a_rfnt = (float)(sup_atten * a_rfnt); /* adjust for attenuator */
}
else
{
    a_rfnt = 0;
}

/* pulse widths and amplitudes for suppression crushers */
pw_gcmt01 = 16ms;
pw_gxcmt01 = pw_gcmt01;
pw_gycmt01 = pw_gcmt01;
pw_gzcmt01 = pw_gcmt01;

pw_gcmt02 = 16ms;
pw_gxcmt02 = pw_gcmt02;
pw_gycmt02 = pw_gcmt02;
pw_gzcmt02 = pw_gcmt02;

pw_gcmt03 = 16ms;
pw_gxcmt03 = pw_gcmt03;
pw_gycmt03 = pw_gcmt03;
pw_gzcmt03 = pw_gcmt03;

if (mtsup_grads == 1)
{

```

```

a_gcmt01 = gmax*cfgcmfs;
a_gcmt02 = gmax*cfgcmfs;
a_gcmt03 = gmax*cfgcmfs;
}
else
{
a_gcmt01 = 0;
a_gcmt02 = 0;
a_gcmt03 = 0;
}

/* toggles to turn crushers on or off */
m_gxcmt01 = 1.0;
m_gycmt01 = 1.0;
m_gzcm01 = 0.0;
m_gxcmt02 = 0.0;
m_gycmt02 = 1.0;
m_gzcm02 = 1.0;
m_gxcmt03 = 1.0;
m_gycmt03 = 0.0;
m_gzcm03 = 1.0;

a_gxcmt01 = a_gcmt01 * m_gxcmt01;
a_gycmt01 = a_gcmt01 * m_gycmt01;
a_gzcm01 = a_gcmt01 * m_gzcm01;

a_gxcmt02 = a_gcmt02 * m_gxcmt02;
a_gycmt02 = a_gcmt02 * m_gycmt02;
a_gzcm02 = a_gcmt02 * m_gzcm02;

a_gxcmt03 = a_gcmt03 * m_gxcmt03;
a_gycmt03 = a_gcmt03 * m_gycmt03;
a_gzcm03 = a_gcmt03 * m_gzcm03;

/* timing for MTsuppression */
/* The wft times are the time taken up by waveforms, the t_ times
are the total times for the interval, and the tstr_ times are
the leftover dead times. All tstr_ times must be >= 0 */

t_mtsp = 1ms;          /* suppression rf/spoiler spacing */
t_mtshimrf = 500us;   /* extra shim time around rf */

/* start to first rf */
wft_mtst01 = pw_rf/2;
t_mtst01 = wft_mtst01 + 2ms;      /* start to center of first rf */
tstr_mtst01 = t_mtst01 - wft_mtst01;

/* center rfmt(n-1) to center rfmt(n) */
wft_mt = pw_rf/2 + t_mtsp + pw_gcmt01 + pw_rf/2;
t_mt = wft_mt + t_mtsp;          /* center rfmt(n-1) to center rfmt(n) */
tstr_mt = t_mt - wft_mt;

/* center rfmt(n-1) to center rfmt(n) => TD */
wft_td = pw_rf/2 + t_mtsp + pw_gcmt01 + pw_rf/2;
td = wft_td + t_mtsp;          /* center rf(n-1) to center rf(n) */
tstr_td = td - wft_td;        /*Observe that if we want different pulsewidths of the crushers, we may have a
problem here*/

/* center rfmt to end */
wft_mtend = pw_rf/2 + t_mtsp + pw_gcmt01;
t_mtend = wft_mtend + t_mtsp;   /* center last rfmt to end of MTsuppression */
tstr_mtend = t_mtend - wft_mtend;

/* total MTsuppression time */
if (mtsup_grads == 1)
t_mtsp = t_label + t_mtst01 + (n_rf - 1) * td + t_mtend;

```

```

else
    t_mtsup = 0;

@pg MTSuppressPG

STATUS MTSuppressPG()
{
int PosTempsup;
int i,j,k;
    /******
Chess suppression rf and crushers
    *****/
if (mtsup_grads == 1)
{
    switch (pulse_rfmt)
    {
        case -1:
            strcpy(fileloc_rfmt, "mtsatslr_1340.rho"); /*slr-pulse*/
            break;
        case 0:
            strcpy(fileloc_rfmt, "mtsatsinc_1620.rho"); /*sinc-pulse*/
            break;
        case 1:
            strcpy(fileloc_rfmt, "mps80_pm_3920.rho");
            break;
        case 2:
            strcpy(fileloc_rfmt, "mps90_pm_3920.rho");
            break;
        case 3:
            strcpy(fileloc_rfmt, "mps100_pm_3920.rho");
            break;
        case 4:
            strcpy(fileloc_rfmt, "mps110_pm_3920.rho");
            break;
        case 5:
            strcpy(fileloc_rfmt, "mps120_pm_3920.rho");
            break;
        case 6:
            strcpy(fileloc_rfmt, "mps130_pm_3920.rho");
            break;
        case 7:
            strcpy(fileloc_rfmt, "mps140_pm_3920.rho");
            break;
    }
i=0;
    for (j = 0; j < n_rf; j++) { /*i=loop-nr, j=rf-nr*/
        if (j == 0) {
            PosTempsup = RDN_GRD(t_stir + t_label + tstr_mtst01 -
                pw_dattenmton);
            SSPPACKET(attenmton01,PosTempsup,pw_dattenmton,dattenmton,0);
            PosTempsup = RUP_GRD(t_stir + t_label + tstr_mtst01);
            temp = PosTempsup;
            shim01out(1);

            PosTempsup = RUP_GRD(pbeg(&gxmtshim01,"gxmtshim01",i) + t_mtshimrf);
            /*PosTempsup = RUP_GRD(t_stir + t_label + tstr_mtst01 + t_mtshimrf);*/
            temp = PosTempsup;
            rfout(1); /*rf01*/
            setrfcontrol(pixmtband,&rfmt);
        }
        if (j % 3 == 0 && j > 0) {
            PosTempsup = RUP_GRD(pend(&gxcmt03,"gxcmt03",i-1) + td - (pw_gxcmt01 + t_mtsp +
                pw_rfmt));
            /*PosTempsup = RUP_GRD(pend(&gxcmt03,"gxcmt03",i-1) + tstr_td);*/

```

```

        temp = PosTempsup - t_mtshimrf;
        shim01out(1);

        temp = PosTempsup;
        rfout(1);                                /*rf-(j+1) rf04,rf07,rf10...*/
        setrfcontrol(pixmtband,&rfmt);
    }

    if (j % 3 == 1){
        PosTempsup = RUP_GRD(pend(&gxcmt01,"gxcmt01",i) + td - (pw_gxcmt02 + t_mtsp + pw_rfamt));
        /*PosTempsup = RUP_GRD(pend(&gxcmt01,"gxcmt01",i) + tstr_td);*/
        temp = PosTempsup - t_mtshimrf;
        shim02out(1);

        temp = PosTempsup;
        rfout(1);                                /*rf-(j+2) rf02,rf05,rf08,rf11...*/
        setrfcontrol(pixmtband,&rfmt);
    }

    if (j % 3 == 2){
        PosTempsup = RUP_GRD(pend(&gxcmt02,"gxcmt02",i) + td - (pw_gxcmt03 + t_mtsp + pw_rfamt));
        /*PosTempsup = RUP_GRD(pend(&gxcmt02,"gxcmt02",i) + tstr_td);*/
        temp = PosTempsup - t_mtshimrf;
        shim03out(1);

        temp=PosTempsup;
        rfout(1);                                /*rf-(j+3) rf03,rf06,rf09,rf12...*/
        setrfcontrol(pixmtband,&rfmt);

        i = i + 1;                                /*"loopnr" tilldelas (index på spoiler och shim)*/
    }

    k = j + 1;
    if (k == n_rf) {
        PosTempsup = RDN_GRD(pend(&rfmt,"rfmt",j) + t_mtsp - pw_dattenmtoff);
        SSPPACKET(attenmtoff,PosTempsup,pw_dattenmtoff,dattenmtoff,0);
    }
    PosTempsup = RUP_GRD(pend(&rfmt,"rfmt",j) + t_mtsp);
    temp = PosTempsup;

    if (j % 3 == 0)
        sinus01out(1);                            /*Första spoilern i varje slinga+Sista spoilern i slingan*/
    if (j % 3 == 1)
        sinus02out(1);
    if (j % 3 == 2)
        sinus03out(1);
}
}
return SUCCESS;
}

```

```
@pg SuppressPG
```

```
STATUS SuppressPG()
{
    int PosTempsup;

```

```
@rsp MTSuppressPsdInit
```

```
/*Sets the frequency for all rfamt-pulses*/
```

```

if (metsup_rf == 1)
{
    int i,j,k,l;
    if (stir == 0)
        for ( i = 0; i < n_rf; i++) {

```

```
        setiamp((SHORT)(ia_rfmt),&rfmt,i);
    }
    if (pixmtband != 1)
    {
        if (stir == 0)
            for (j = 0; j < n_rf; j++) {
                setiphase(max_pg_wamp/2,&rfmt,j);
            }
    }
    else
    {
        if (stir == 0)
            for (k = 0; k < n_rf; k++) {
                setiphase(-max_pg_wamp/2,&rfmt,k);
            }
    }

    if (stir == 0)
        for (l = 0; l < n_rf; l++) {
            setfrequency(freq_inv*rfmt_freq,&rfmt,l);
        }
}
```

10. List of Abbreviations

CW	Continuous Wave
EC	Extra Cellular Water
FLASH	Fast Low Angle SHot
IC	Intra Cellular Water
MS	Multiple Sclerosis
MT	Magnetic Transfer
MTR	Magnetic Transfer Ratio $(M_z - M_0)/M_0$. The percent magnetisation transferred
MTR(TD)	MTR steady state value for pulsed saturation transfer experiment with the distance TD between the pulses
MTR _{CW}	MTR steady state value for continuous wave saturation transfer experiment
PRESS	Point RESolved Spectroscopy
SAR	Specific Absorption Rate.
STEAM	STimulated Echo Acquisition Mode
TD	Time Delay between the pulses in the saturation pulse train.
TR	Time of Repetition (Time between two excitation of the same volume)
VOI	Volume Of Interest

11. Acknowledgements

I wish to thank Ph.D. Gunther Helms for his support and never ending enthusiasm in this work. He should also have all credits for the dynamic evaluation of pulsed MT. I also want to thank Stefan Skare and Magnus Karlsson for the support. I also wish to thank the opponent Peter Lundberg of Linköping University for stimulating comments and reviewing the manuscript.

Finally I would like to thank the personal at MRC for their help and most stimulating and “relaxing” coffee breaks.

12. References

- 1) Forsen S, Hoffman RA: Study of moderately rapid chemical exchange reactions by means of nuclear magnetic double resonance. *Journal Chem. Phys.* 1963; 39:2892-2901.
- 2) Roland Kreis, Ph.D. : ^1H MR Spectroscopy: Methods and Applications.
- 3) Gunther Helms: Radiofrequency Pulse in der lokalisierten STEAM-Spektroskopie.
- 4) John Eng et al. Quantitative ^1H Magnetization transfer Imaging in vivo. *Magnetic Resonance In Medicine* 17,304-314(1991).
- 5) R C Metha et al. Magnetization Transfer MR of the normal Adult Brain. *AJNR Am J Neuroradiol* 16:2085-2091, Nov 1995.
- 6) Siemens. Magnetization Transfer Saturation.
- 7) Raimo Sepponen: Rotating frame and Magnetization Transfer ,chapter 8.
- 8) G. Bruce Pike et al: Pulsed Magnetization Transfer Spin Echo MR Imaging. *JMRI* 1993;3:531-539
- 9) R. Mark Henkelman et al: Quantitative Interpretion of Magnetization Transfer. *MRM* 29:759-766 1993
- 10) Clare Morrison, R. Mark Henkelman: A model for Magnetization Transfer in Tissues. *MRM* 33:475-482 1995.
- 11) Steven D. Wolff, Robert S. Balaban: Magnetization Transfer Contrast(MTC) and Tissue Water Proton Relaxation in Vivo. *Magnetic Resonance In Medicine* 10, 135-144(1989).
- 12) Bob s. Hu et al: Pulsed Saturation transfer Contrast. *Magnetic Resonance In Medicine* 26, 231-240(1992).
- 13) G.Bruce Pike: Pulsed Magnetization Transfer Contrast in Gradient Echo Imaging: A two pool analytic Description of Signal Responce. *MRM* 36:95-103(1996)
- 14) Steven Wolff, Robert S. Balaban: Magnetization transfer Imaging: Practical Aspects and Clinical Applications. *Radiology* 1994;192:593-599.
- 15) T.Ernst et. al. *JMR Series B* 102,1-8 (1993).Absolute Quantitation of Water and Metabolites in the Human Brain. 1.Compartments of Water.

- 16) Jonathan G. Li, R. Mark Henkelman. MRM 37:866-871(1997).A Flexible Magnetisation Transfer Line Shape Derived from Tissue Experimental data.
- 17) G. Helms. A complete and Unbiased Sensitivity Correction Based on the Localised Signal for Absolute Quantification of Proton MRS Data of The Human Brain *In Vivo*.

Theoretically, the time dependent parameters μ_1 and μ_2 can be determined by curve fits of the measurement described in fig. 7.4. However, the small number of measure points results in too uncertain values of μ_2 and therefore the μ_1 values are only to be considered in our measurements. As seen in fig. 7.6 the μ_1 dependence for white matter corresponds well to the theoretical model, whereas the fit of grey matter is not as good.

Possible improvement through better hardware should allow the preparation time to be longer and the RF-amplifier software should be changed to better fit the duty cycle of the RF-amplifier, resulting in a fully achieved steady state.

These limitations gave us severe problems reaching steady state. Possible improvement through better hardware should allow the preparation time to be longer and the RF-amplifier software should be changed to better fit the duty cycle of the RF-amplifier, resulting in a fully achieved steady state.